9 Similarity Theory

For a number of boundary layer situations, our knowledge of the governing physics is insufficient to derive laws based on first principles. Nevertheless, boundary layer observations frequently show consistent and repeatable characteristics, suggesting that we could develop empirical relationships for the variables of interest. Similarity theory provides a way to organize and group the variables to our maximum advantage, and in turn provides guidelines on how to design experiments to gain the most information.

9.1 An Overview

9.1.1 Definitions and Methodology

Similarity theory is based on the organization of variables into ***dimensionless groups***. Fortunately, there is a ***dimensional-analysis*** procedure called ***Buckingham Pi theory*** that aids us in forming dimensionless groups from selected variables. It is hoped that the proper choice of groups will allow empirical relationships between these groups that are "***universal***" — namely, that work everywhere all the time for the situation studied.

The four steps in developing a similarity theory are:

(1) select (guess) which variables are relevant to the situation,
(2) organize the variables into dimensionless groups,
(3) perform an experiment, or gather the relevant data from previous experiments, to determine the values of the dimensionless groups,
(4) fit an empirical curve or regress an equation to the data in order to describe the relationship between groups.

The result of this four-step process is an empirical equation or a set of curves which show the same shape — in other words the curves look self similar. Hence, the name ***similarity theory***. If this empirical result is indeed universal, then we can use it on days and locations other than those of the experiment itself. Such expectations should be tested with an independent data set, before the results are disseminated to the rest of the scientific community.

If we selected in step (1) more variables than were necessary, the data will "tell us" of our mistake by indicating no change of the other dimensionless groups with respect to the group that is irrelevant. If we selected too few variables, or excluded an important variable, the data will also indicate our error by showing a large scatter or no repeatable patterns between the dimensionless groups.

Step (2) can often be performed by inspection of the relevant variables. In fact, based on the classes of similarity theory frequently used in meteorology (see Section 9.3.3), we can anticipate the dimensionless groups, although we can not always anticipate the relationship between the groups. For the very complex problems, we can employ Buckingham Pi Theory to identify the appropriate dimensionless groups.

Similarity theory does not tell us the form of the equation or the relationship between the dimensionless groups. Instead, we must use trial and error, physical insight, or automated techniques to select the form that qualitatively "looks the best". For example, we might express one group as a power law function of another group, as a logarithmic relationship, or as a constant that is not a function of other groups. The chosen equation usually contains unknown coefficients, which can then be solved by regression against the observed data.

The resulting equations are called ***similarity relationships (or relations),*** or sometimes, improperly, ***similarity laws.*** Frequently, the dimensionless data graphs or curves are presented without a corresponding regression equation, because no simple equation could be found. For these cases, one can use the graph directly to determine the value of one dimensionless group as a function of the values of the other groups. We ***normalize*** an important variable when we divide it by other variables to make it dimensionless; hence, these graphs represent normalized data.

Similarity relationships are usually designed to apply to ***equilibrium*** (steady-state) situations. They are frequently used to yield equilibrium profiles of mean variables and turbulence statistics as a function of height or position. Rarely is time included as one of the relevant variables. Some variables, such as depth of the boundary layer, are so strongly dependent on time that no successful similarity expressions have been found to diagnose them. Instead, boundary layer depth must be calculated or measured using other techniques. This depth is used as input into dimensionless groups to diagnose other variables that do reach a quasi-steady state.

Finally, similarity theory is a type of zero-order closure. Once the similarity relationships have been identified, they can be used to diagnose equilibrium values of mean wind, temperature, moisture, and other variables as a function of height without any turbulence closure assumptions being made.

9.1.2 Example

Problem. Find a similarity relationship for the buoyancy flux, $\overline{w'\theta_v'}$, as a function of height in the convective mixed layer.

Solution. First (step 1), guess the relevant variables. Based on the problem statement, we already know that two of the variables of interest are $\overline{w'\theta_v'}$ and z. The depth of the mixed layer, z_i, and the strength of the heat flux near the surface, $\overline{w'\theta_v'}_s$, might also influence the flux within the interior of the mixed layer. Thus, we will use four variables for this analysis.

Step (2), group these four variables into dimensionless groups. By inspection, we can easily produce two dimensionless groups: $[z/z_i]$ and $[\overline{w'\theta_v'} / \overline{w'\theta_v'}_s]$. We have thus reduced our degrees of freedom from four to two.

In performing our experiment for step (3), dimensional analysis tells us that we need not measure all combinations of z, z_i, $\overline{w'\theta_v'}$, and $\overline{w'\theta_v'}_s$. Instead, we need only measure various combinations of the two groups: $[z/z_i]$ and $[\overline{w'\theta_v'} / \overline{w'\theta_v'}_s]$. This greatly simplifies the design and conduct of our experiment.

Suppose the heat flux data from Fig 3.7 (reproduced as Fig 9.1a) represents the results of our experiment. The curves in this data set exhibit a common shape: there is a nearly-linear decrease of heat flux from the surface value to a small negative value near the top of the mixed layer. Above that, the flux reduces toward zero. As we shall soon learn in Chapter 11, the average depth of the mixed layer is frequently taken as the height where the heat flux is most negative. When each of the data curves is replotted in terms of the two dimensionless groups, as shown in Fig 9.1b, we happily find that all of the data is closely clustered around a single curve.

For step (4), an obvious choice of curve is a straight line between the surface and the top of the mixed layer. By definition we want the intercept of this line to equal 1, and by inspection it looks like the slope is roughly 1.2. This results in:

$$\frac{\overline{w'\theta_v'}}{\overline{w'\theta_v'}_s} = 1 - 1.2\left[\frac{z}{z_i}\right] \qquad \text{for } 0 \le (z/z_i) \le 1$$

which is also plotted in Fig 9.1b. As an independent test, the buoyancy flux data from Figs 3.1b, 3.2b, and 3.3b confirm the validity of our curve.

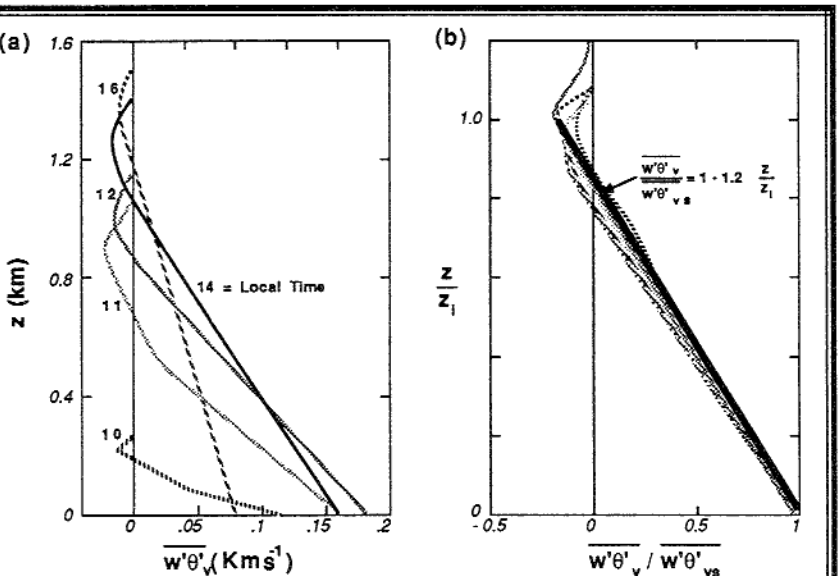

Fig. 9.1 Raw heat flux data from a simulation of Wangara Day 33 (a) replotted in a dimensionless framework (b). The empirical straight line estimate from similarity theory is also shown in (b).

Discussion. We hope to be able to use this equation to diagnose the value of the buoyancy flux at any height within the interior of a convective mixed layer on any other day at any other location, assuming we know the surface flux and the mixed layer depth. Even without this equation, we could use Fig 9.1b to determine the flux at any height.

For example, suppose the aircraft-measured buoyancy flux of $\overline{w'\theta_v'} = 0.1$ K·ms^{-1} at a height of $z = 200$ m when the mixed layer depth was $z_i = 1300$ m. We can used this data along with the similarity relation above to estimate the surface buoyancy flux: $\overline{w'\theta_{v\,s}'}$ = 0.123 K·ms^{-1}.

9.2 Buckingham Pi Dimensional Analysis Methods

In 1914 Buckingham proposed a systematic approach for performing dimensional analysis. He called the resulting dimensionless groups ***Pi groups***, which later caused the theory to be known as Buckingham Pi Theory (Perry, et al., 1963).

For each step of his approach we will first define the general procedure (in ***boldface***), and then give an example (in normal type face). The example is that of fluid flow through a pipe, and involves the question: "How does the shear stress, τ, vary?"

Step 1. Hypothesize which variables could be important to the flow.
Example: stress, density, viscosity, velocity, pipe diameter, pipe roughness

Step 2. Find the dimensions of each of the variables in terms of the fundamental dimensions. The fundamental dimensions are:

L = length
M = mass
T = time
K = temperature
A = electric current
I = luminous intensity

The dimensions of any variable can be broken into these fundamental dimensions.

Example:

variable	name	fundamental dimensions
ρ	fluid density	$M L^{-3}$
μ	dynamic viscosity	$M L^{-1} T^{-1}$
U	velocity	$L T^{-1}$
τ	shear stress	$M L^{-1} T^{-2}$
D	pipe diameter	L
z_o	pipe roughness length	L

The first two variables describe fluid characteristics, the next two describe flow characteristics, and the last two describe pipe characteristics.

Step 3: Count the number of fundamental dimensions in our problem.
Example: There are 3 dimensions: L, M, T.

Step 4: Pick a subset of your original variables to become "key variables", subject to the following restrictions:

(a) The number of key variables must equal the number of fundamental dimensions.

(b) All fundamental dimensions must be represented in the key variables.

(c) No dimensionless group must be possible from any combination of these key variables.

Example: Pick 3 variables: ρ, D, and U to be the key variables.
Note that there are many other equally valid choices for key variables, such as: ρ, z_o, U; or τ, μ, D, etc. It does not matter which three are picked, assuming that all of the above restrictions are satisfied. An invalid set would be U, D, z_o, because D/z_o is dimensionless, and also because the fundamental dimension M is not represented. Another invalid set is τ, ρ, U, because $\tau/(\rho U^2)$ is dimensionless.

Step 5. Form dimensionless equations of the remaining variables in terms of the key variables.

Example: $\tau = (\rho)^a\ (D)^b\ (U)^c$

$\mu = (\rho)^d\ (D)^e\ (U)^f$

$z_o = (\rho)^g\ (D)^h\ (U)^i$

where a-i are unknown powers.

Step 6. Solve for the powers a, b, c, . . . to yield dimensionally consistent equations.

Example: Solve each equation independently. For the first equation:

$$\tau = (\rho)^a\ (D)^b\ (U)^c$$

or $$M\,L^{-1}\,T^{-2} = (M\,L^{-3})^a\,(L)^b\,(L\,T^{-1})^c$$

or $$M\,L^{-1}\,T^{-2} = M^a\ \ L^{-3a+b+c}\ \ T^{-c}$$

The dimensions on the left hand side must equal the dimensions on the right. Thus:

M: $1 = a$

L: $-1 = -3a + b + c$

T: $-2 = -c$

These three equations can be solved for the three unknowns, yielding:

$a = 1 \qquad b = 0 \qquad c = 2$.

Thus, a dimensionally consistent equation is: $\tau = (\rho)^1\ (D)^0\ (U)^2$, or $\tau = \rho\,U^2$.

Similarly, we find that $d = 1$, $e = 1$, $f = 1$: yielding $\mu = \rho\,U\,D$.

Also: $g = 0$, $h = 1$, $i = 0$: yielding $z_o = D$.

Step 7. For each equation, divide the left hand side by the right hand side to give dimensionless (Pi) groups. The number of Pi groups will always equal the number of variables minus the number of dimensions.

Example:

$$\pi_1 = \frac{\tau}{\rho\,U^2} \qquad \pi_2 = \frac{\mu}{\rho\,U\,D} \qquad \pi_3 = \frac{z_o}{D}$$

We started with 6 variables in our example, and reduced our degrees of freedom down to 3 dimensionless groups.

Step 8. (Optional) If desired, alternative Pi groups can be formed from the ones derived in the previous step, as long as: the total number of Pi groups does not change, all variables are represented, and no one Pi group can be formed from any combination of the remaining groups.

Example: One alternative set of Pi groups might be: π_1, π_4 $(=\pi_2/\pi_3)$, π_5 $(=1/\pi_3)$.

This new set is:

$$\pi_1 = \frac{\tau}{\rho U^2} \qquad \pi_4 = \frac{\mu}{\rho U z_o} \qquad \pi_5 = \frac{D}{z_o}$$

In fact, regardless of which set of primary variables were chosen, we can always arrive at the same set of Pi groups via this Pi-group manipulation process.

You might ask which set of Pi groups is the "correct" set. They are all equally valid, although some Pi groups have become more popular than others in the literature. Our pipe example is a case in point. We can recognize π_1 as identical to the definition of ***drag coefficient***, C_D, while π_2 is just the inverse of the ***Reynolds number***, Re $= \rho U D / \mu$. The π_3 group is called the ***relative roughness***.

This is the end of the formal cookbook procedure for Buckingham Pi Theory. Of course, it is really only the second step of the overall similarity procedure. The next step would be to perform the necessary experiments to discover the relationships between the Pi groups. An example of laboratory pipe flow data is shown in Fig 9.2.

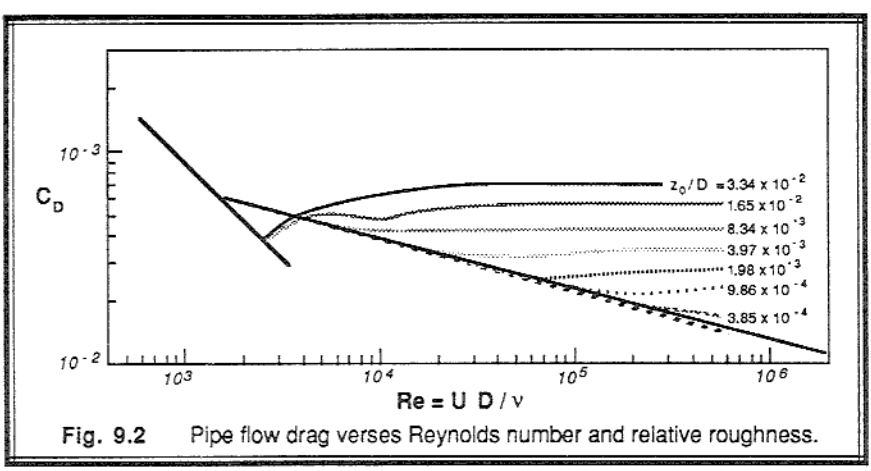

Fig. 9.2 Pipe flow drag verses Reynolds number and relative roughness.

Discussion: Several very important facts can be learned from this data. First, the stress decreases as the Reynolds number increases, until a critical Reynolds number of about 2100 is reached. This critical Reynolds number marks the transition from laminar to turbulent flow. At lower Reynolds number (laminar flow), the stress is NOT dependent on the relative roughness. As suggested in Section 9.1, the data is telling us that pipe roughness is not relevant for laminar flow.

Second, at Reynolds numbers just larger than critical, the stress increases again. Third, as Reynold's number increases further, the stress again decreases with Reynolds

number, independent of the pipe roughness. Fourth, this roughness independence fails when some ***roughness Reynolds number*** (given by π_4) is reached. Fifth, at even larger Reynolds number, the stress is a constant depending only on relative roughness and not on the Reynolds number itself.

This last observation is of important consequence for the atmosphere. As previously discussed, the Reynolds number for the atmosphere is very large, on the order of 10^6 to 10^8, even within the boundary layer. Fig 9.2 shows us that ***large Reynolds number flow*** is independent of the Reynolds number! Hence, we can usually ignore molecular viscosity and the associated Reynolds number in descriptions of the boundary layer. However, for the very smallest size eddies and in the very thin microlayer near the surface, molecular viscosity continues to be important for TKE dissipation and transport across the surface, respectively.

9.3 Scaling Variables

9.3.1 Choice of Key Variables

Within the constraints of Buckingham Pi theory, there is a wide variety of variables that could be chosen as the key variables. Usually, it is better to pick variables that represent forcings on the boundary layer, or variables that reflect aspects of the non-steady condition of the boundary layer. For example, most surface fluxes represent forcings that are (partially) controlled by external factors. The depth of the boundary layer, as mentioned before, is one important non-steady condition of the boundary layer.

9.3.2 Lists of Scaling Variables

Experience has shown that some key variables frequently appear in common classes of similarity problems, and hence are known as ***scaling variables*** for that class. As you might guess, a large variety of scaling variables have been suggested over the years (see Table 9-1). In any dimensional analysis problem, you must select only those scales appropriate to the situation. Recommendations for relevant scales were given in Figs. 5.26 and 5.27. Usually, you should pick only one length scale, one velocity scale, and if needed one temperature scale and one humidity scale to be your key variables. No time scale is usually picked, because a time scale can be formed from the length and velocity scales.

9.3.3 Combining Variables to Make New Scales

Some variables always appear grouped in the same arrangements, allowing us to define new scaling variables based on the combination of variables. For example, we have already encountered the friction velocity and other scales in Section 2.10 for the class of problems relating to the surface layer. In Section 4.2 we discussed the convective velocity and other scales related to the class of mixed-layer problems.

Table 9-1. Summary of boundary layer scales.

Length:	z	= height above the surface
	h or z_i	= depth of the boundary layer (or mixed layer)
	H	= SBL integral length scale = heat-flux-history scale
	L	$= -[\overline{u'w'}_s^2 + \overline{v'w'}_s^2]^{3/4}/[k\cdot(g/\overline{\theta_v})\cdot(\overline{w'\theta_v'}_s)]$ = Obukhov length
	L_L	$=-[\overline{u'w'}^2+\overline{v'w'}^2]^{3/4}/[k\cdot(g/\overline{\theta_v})\cdot(\overline{w'\theta_v'})]$ =local Obukhov length
	h_e	$= u_*/f_c$ = Ekman layer depth
	λ_{max}	= Wavelength corresponding to peak in turbulence spectrum
	H	= height of obstacle
	W	= width of obstacle
	z_o	= aerodynamic roughness length
	Z_s	= scale of surface features or roughness
Velocity:	u_*	$= [\overline{u'w'}_s^2 + \overline{v'w'}_s^2]^{1/4}$ = friction velocity
	w_*	$= [(g/\overline{\theta_v})\cdot\overline{w'\theta_v'}_s\cdot z_i]^{1/3}$ = convective velocity scale
	w_{Lf}	$= [(g/\overline{\theta_v})\cdot\overline{w'\theta_v'}\cdot z]^{1/3}$ = local free convection velocity scale
	u_L	$= [\overline{u'w'}^2+\overline{v'w'}^2]^{1/4}$ = local (friction) velocity scale
	V_B	$= [(g/\Delta\overline{\theta_v}_s)\cdot\overline{w'\theta_v'}\cdot H]^{1/3}$ = SBL buoyancy velocity scale
	V_M	$= (Z_s/\rho)^{1/2}[(\partial P/\partial x)^2+(\partial P/\partial y)^2]_s^{1/4}$ = mechanical forcing scale
	u_*^{ML}	$= u_*^2/w_*$ = convective stress scale velocity
	$\overline{G}$ or $\overline{U_g}$	= geostrophic wind speed
	$\overline{G}_s$	= geostrophic wind speed at the surface
	$\overline{G}_{z_i}$	= geostrophic wind at the top of the boundary layer
	$\langle\overline{G}\rangle$	= geostrophic wind speed averaged over the boundary layer
	$\overline{U}$ or $\overline{M}$	= wind speed
	$\overline{M}_S$	= wind speed at the surface

$\overline{M}_{z_i}$ = wind speed at the top of the boundary layer

$\langle\overline{M}\rangle$ = wind speed averaged over the boundary layer

s_u or σ_u = standard deviation of U-wind

$(TKE)^{1/2}$ or $\bar{e}^{1/2}$ = square root of turbulence kinetic energy

$(k\, z\, \varepsilon)^{2/3}$ = dissipation velocity scale in the surface layer

Time:

$1/f_c$ = inertial period, where f_c is the Coriolis parameter

$1/N_{BV}$ = buoyant period, where N_{BV} is the Brunt-Väisälä frequency

$1/f_{max}$ = eddy period, where f_{max} is the frequency at the peak in the turbulence spectrum

t_*^{ML} = z_i / w_* = convective (ML) time scale

t_*^{SL} = z / u_* = surface-layer time scale

$x/\overline{U}$ = time required for wind to move distance x

Temperature:

θ_*^{ML} = $\overline{w'\theta_v'}_s / w_*$ = convective (ML) temperature scale

θ_*^{SL} = $-\overline{w'\theta_v'}_s / u_*$ = surface-layer temperature scale

θ_{Lf} = $\overline{w'\theta_v'} / w_{Lf}$ = local free-convection temperature scale

θ_L = $-\overline{w'\theta_v'} / u_L$ = local temperature scale

θ_* = $\overline{w'\theta_v'}_s$ /(any other velocity scale)

$\langle\overline{\theta_v}\rangle$ = mixed-layer average of $\overline{\theta_v}$

$\Delta\theta_s$ = $\langle\overline{\theta_v}\rangle - \overline{\theta}_{vs}$ = SBL surface cooling (inversion strength)

Moisture:

q_*^{ML} = $\overline{w'q'}_s / w_*$ = convective (ML) humidity scale

q_*^{SL} = $-\overline{w'q'}_s / u_*$ = surface-layer humidity scale

q_{Lf} = $\overline{w'q'} / w_{Lf}$ = local free-convection humidity scale

q_L	$= -\overline{w'q'}/u_L$ = local humidity scale
q_*	$= \overline{w'q'}_s$ /(any other velocity scale)

As an example of the power of combining variables into new scales, we might expect z_i, $\overline{w'\theta_v'}_s$, and maybe $g/\overline{\theta_v}$ to always be important in convection, because heating, convection, and buoyancy cause thermals to rise to the top of the mixed layer. In fact, these key variables are often grouped as $[(g/\overline{\theta_v})\cdot\overline{w'\theta_v'}_s \cdot z_i]$ during a dimensional analysis. We recognize this group to be the basis for the definition of the convective velocity scale w_*; namely, $w_*^3 = [(g/\overline{\theta_v})\cdot\overline{w'\theta_v'}_s \cdot z_i]$ as defined in Section 4.2.

By using such a scaling variable in dimensional analysis, we can often reduce the total number of variables in our problem and greatly simplify the analysis. For example, if we wish to find a relationship for $\overline{w'^2}$ as a function of height in the ML, we might choose $\overline{w'^2}$, z, $\overline{w'\theta_v'}_s$, z_i, and $g/\overline{\theta_v}$ as the relevant variables for the first step in the analysis. Alternately, by using the combined scaling variables, we would choose $\overline{w'^2}$, w_*, z, and z_i instead. With this last set of variables, we can easily identify the dimensionless groups by inspection: $[\overline{w'^2}/w_*^2]$ and $[z/z_i]$.

9.3.4 Classes of Similarity Scales

The most common classes of similarity scaling are ***Monin-Obukhov similarity, mixed-layer similarity, local similarity, local free convection,*** and ***Rossby-number similarity***. When dealing with one of these well-defined classes of problems, it is appropriate to use the associated scaling variables as the key variables in a dimensional analysis.

Monin-Obukhov Similarity. This class is usually applied to the surface layer (Monin and Obukhov, 1954; Wyngaard, 1973; Sorbjan, 1986), and hence is sometimes called ***surface-layer similarity***. Earlier we defined the surface layer as that part of the boundary layer where the fluxes vary by less than 10% of their magnitude with height. To a first order approximation, this layer is a ***constant flux layer***. We can thus

simplify our description of the surface layer by utilizing the flux at just one height — usually the surface.

Monin-Obukhov similarity works only when the winds are not calm, and u_* not zero. Relevant scales based on these surface fluxes and their typical orders of magnitude are listed here:

L	Order (1 m to 200 m)
z_o	Order (1 mm to 1 m)
u_*	Order (0.05 to 0.3 m/s)
θ_*^{SL}	Order (0.1 to 2.0 °C)
q_*^{SL}	Order (0.1 to 5 g_{water}/kg_{air})

Scales for pollutant concentration can be patterned after the humidity scale. Lists of Monin-Obukhov similarity relationships are tabulated in Sections 9.4 to 9.6, and a more detailed analysis of the log-wind profile in the surface layer is given in Section 9.7.

Mixed-Layer Similarity. This class is applied to mixed layers that are in a state of free convection (Deardorff, 1972; Deardorff, et al., 1980; Sorbjan, 1986), assuming calm or light winds. Free convection conditions can occur during cold air advection over a warmer surface, or with solar heating of the land during the daytime in light wind conditions. The relevant scales and typical orders of magnitude for the mixed layer are:

z_i	Order (0.2 to 2 km)
w_*	Order (2 m/s)
θ_*^{ML}	Order (0.1 K)
q_*^{ML}	Order (0.1 g/m^3)
u_*^{ML}	Order (0.02 m/s)

Other scales, such as for pollutant concentration, can be defined in analogy to the moisture scale. More details are discussed in Section 9.6.

Local Similarity. For statically stable boundary layers, this class recognizes that turbulence in the mid and upper SBL may not be in equilibrium with the surface fluxes (Wyngaard, 1973; Nieuwstadt, 1984; Sorbjan, 1987). Hence, local fluxes, shears and stability are more important than surface fluxes. The relevant scales are:

L_L	Order (0 to 50 m)
u_L	Order (0 to 0.3 m/s)
θ_L	Order (0 to 2.0 °C)
q_L	Order (0 to 5 g_{water}/kg_{air})

Dimensionless groups formed with the above scales are not a function of height above ground; hence, this scaling is also called ***z-less*** scaling. Although the dimensionless groups are independent of height, the individual variables that make up these groups (including the scaling variables above) vary significantly with height.

Local Free Convection Similarity. In statically unstable surface layers, buoyancy is the driving force behind the turbulence. However, turbulence in the surface layer might "feel" the influence of the ground more than the influence of the capping inversion (Wyngaard, et al., 1971; Tennekes, 1973; Wyngaard, 1973; Caughey and Palmer, 1979; Sorbjan, 1986). As a result, z_i is not a relevant parameter, but z is. The list of relevant scales becomes:

z	Order (0 to 50 m)
w_{Lf}	Order (0 to 0.5 m/s)
θ_{Lf}	Order (0 to 2.0 °C)
q_{Lf}	Order (0 to 5 g_{water}/kg_{air})

This similarity approach is useful for surface layers in conditions of calm mean winds. In that case the Obukhov length is zero, and is not an appropriate measure of the amount of turbulence being generated. Thus, Monin-Obukhov similarity will not work.

Rossby-number Similarity. In some situations such as large-scale modeling, it is desirable to relate surface fluxes to external forcings. In this regard, it is necessary to ***match*** the wind and temperature profiles higher in the boundary layer with those in the surface layer (Tennekes, 1973; Yamada, 1976). As a result, relevant scales include both surface scales (z_o, L, u_*, θ_*^{SL}, q_*^{SL}) and scales appropriate to the upper boundary layer (h_2, G_2, θ_2, q_2).

In early work (see review by Tennekes, 1982), it was suggested that the h_2 scale be described by G/f_c. When this "outer" scale is combined with the "inner" scale, z_o, the result is the ***surface Rossby number***, $G/(f_c z_o)$. Unfortunately, this approach was not completely successful, resulting in a search for better outer scales. Although still not perfect, the following outer scales are now more widely accepted (z_i , <G>, $\Delta\theta_s$, Δq_s). Details of this approach are reviewed in Section 9.8.

9.3.5 Similarity Relationships

Many of the figures in Chapters 4 and 5 are already presented in similarity form using the above scales, with one dimensionless group plotted as a function of other dimensionless groups. These curves represent graphical representations of similarity relationships, and can be used directly to estimate the values of variables at any height, within the limitations of the data (e.g., free convection within the mixed layer). Similarity graphs are presented for unstable, neutral and stable boundary layers in those chapters.

Analytical equations have been suggested in the literature for some of the graphical similarity results. In some of these cases, curves are fit to only a subdomain of the turbulence, or apply under only certain conditions. Many of the analytical similarity relationships that have proved successful are summarized in Sections 9.4 through 9.6.

We will start in Section 9.4 by listing similarity relationships for stable (nocturnal) boundary layers, and then proceed to the neutral and unstable (convective) boundary layers in Sections 9.5 and 9.6, respectively. Subsections for mean variables, fluxes,

variances, and other miscellaneous variables will be presented. Each of these subsections will include relationships for both the boundary layer, and the surface layer.

Occasionally, different investigators have suggested different values for the regression coefficients (i.e., the universal constants). For these situations a variety of values are listed, separated by commas.

Finally, an example will be presented in each Section to demonstrate the application of a similarity relationship.

9.4 Stable Boundary Layer Similarity Relationship Lists

In the stable surface layer, Monin-Obukhov similarity has allowed us describe the vertical profiles of some variables as a function of the dimensionless group z/L (Businger, et al., 1971; Wyngaard, et al., 1971; Caughey, et al., 1979). Higher in the SBL, z-less scaling is more appropriate (Wyngaard, 1973; Nieuwstadt, 1984; Lascer and Arya, 1986; Sorbjan, 1986, 1987). Sorbjan (1987) has shown how it is possible to develop SBL similarity expressions from the corresponding surface layer expressions.

All of these relationships assume that the SBL is continuously turbulent in time and space, with no gaps or patches of nonturbulent air. Since real SBLs can have sporadic, patchy turbulence, we must recognize the limitations of the expressions below.

9.4.1 Mean Variables and Their Gradients

In many cases it is difficult to describe the profiles of mean variables because of the influence of initial and boundary conditions. However, the profiles often exhibit a common shape, allowing similarity expressions to be derived for the gradients of mean variables.

Boundary-Layer Relationships:

$$\frac{k L_L}{u_L}\left[\left(\frac{\partial \overline{U}}{\partial z}\right)^2+\left(\frac{\partial \overline{V}}{\partial z}\right)^2\right]^{1/2} = 2.5, \quad 4.7, \quad 5.22 \qquad (9.4.1a)$$

$$\frac{k L_L}{\theta_L}\frac{\partial \overline{\theta}}{\partial z} = 4.23, \quad 4.7, \quad 5.0 \qquad (9.4.1b)$$

Surface-Layer Relationships:

$$\phi_M = \frac{k z}{u_*}\left[\left(\frac{\partial \overline{U}}{\partial z}\right)^2+\left(\frac{\partial \overline{V}}{\partial z}\right)^2\right]^{1/2} = 1 + 4.7\frac{z}{L} \qquad (9.4.1c)$$

$$\phi_H = \frac{k\,z}{\theta_*^{SL}} \frac{\partial \bar{\theta}}{\partial z} = 0.74 + 4.7 \frac{z}{L} \qquad (9.4.1d)$$

These last two expressions are known as ***Businger-Dyer flux-profile relationships***, because they relate mean profile gradients to the fluxes in u_* and θ_*^{SL}. These relationships are plotted in Fig 9.9, and are discussed in more detail in Section 9.7.

9.4.2 Fluxes

Boundary-Layer Relationships:

$$\frac{\overline{u'v'}}{u_L^2} = -1.0 \qquad (9.4.2a)$$

$$\frac{\left[\overline{u'\theta'}^2 + \overline{v'\theta'}^2\right]^{1/2}}{u_L\,\theta_L} = 3.5, \quad 4.0, \quad 5.0 \qquad (9.4.2b)$$

The above expressions are z-less. In order to make these more useful, some parameterizations have been proposed for the fluxes upon which u_L and q_L are based:

$$\frac{-\overline{u'w'}}{u_*^2} = 1 - \left(\frac{z}{h}\right)^{0.7} \qquad (9.4.2c)$$

$$\frac{-\overline{u'w'}}{u_*^2} = \left[1 - \frac{z}{h}\right]^{1 \text{ or } 2} \qquad (9.4.2d)$$

$$\frac{\overline{w'\theta'}}{\overline{w'\theta'}_s} = \left[1 - \left(\frac{z}{h}\right)^{0.5}\right]^{1.5} \qquad (9.4.2e)$$

$$\frac{\overline{w'\theta'}}{\overline{w'\theta'}_s} = \left[1 - \frac{z}{h}\right]^{1 \text{ to } 3} \qquad (9.4.2f)$$

$$\frac{-\overline{u'\theta'}}{\overline{w'\theta'}_s} = 3.2\left[1 - \left(\frac{z}{h}\right)^{0.7}\right]^{1.7} \qquad (9.4.2g)$$

These last five expressions are obviously not z-less, and are likely to be valid for only a small subset of real SBLs.

Surface-Layer Relationships:

$$\frac{\overline{u'v'}}{u_*^2} = \text{constant} \qquad (9.4.2h)$$

$$\frac{\left(\overline{u'\theta'}^2 + \overline{v'\theta'}^2\right)^{1/2}}{u_* \, \theta_*^{SL}} = 4 \qquad (9.4.2i)$$

9.4.3 Variances

Boundary-Layer Relationships:

$$\frac{\left[\overline{u'^2} + \overline{v'^2}\right]^{1/4}}{u_L} = 2.6, \quad 3.1, \quad 4 \qquad (9.4.3a)$$

$$\frac{\left[\overline{w'^2}\right]^{1/2}}{u_L} = 1.5, \quad 1.6, \quad 2.0 \qquad (9.4.3b)$$

$$\frac{\left[\overline{\theta'^2}\right]^{1/2}}{\theta_L} = 2.4, \quad 3.5, \quad 4.0 \qquad (9.4.3c)$$

$$\frac{\bar{e}}{u_L^2} = \text{constant} \qquad (9.4.3d)$$

As before, the above z-less expressions are difficult to use unless the local scaling

variables are known as a function of height. As an alternative, the following height-dependent relationships have been suggested:

$$\frac{\overline{u'^2}}{u_*^2} = 6\left[1 - \left(\frac{z}{h}\right)^{1/2}\right] \qquad (9.4.3e)$$

$$\frac{\overline{w'^2}}{u_*^2} = 2.5\left[1 - \left(\frac{z}{h}\right)^{0.6}\right] \qquad (9.4.3f)$$

$$\frac{\overline{\theta'^2}}{\theta_*^{SL\,2}} = 6.0\left[1 - \left(\frac{z}{h}\right)^{0.4}\right]^{1.5} \qquad (9.4.3g)$$

Surface-Layer Relationships:

$$\frac{\overline{u'^2} + \overline{v'^2}}{u_*^2} = 8.5 \qquad (9.4.3h)$$

$$\frac{\overline{w'^2}}{u_*^2} = 2.5 \qquad (9.4.3i)$$

$$\frac{\overline{\theta'^2}}{\theta_*^{SL\,2}} = 4.0 \qquad (9.4.3j)$$

$$\frac{\bar{e}}{u_*^2} = \text{constant} \qquad (9.4.3k)$$

9.4.4 Miscellaneous

Boundary-Layer Relationships:

$$\frac{k L_L \varepsilon}{u_L^3} = 3.7 \qquad (9.4.4a)$$

Surface-Layer Relationships:

$$\frac{k L \varepsilon}{u_*^3} = 3.7 \qquad (9.4.4b)$$

9.4.5 Example

Problem: Find the local value of the heat flux at a height of $z = 50$ m in a SBL, where the local lapse rate is 0.025 K/m and the local scaling velocity is $u_L = 0.1$ m/s.

Solution: Equation (9.4.1b) can be manipulated, using the definition for L_L, to read

$$\overline{w'\theta'}^2 = \frac{u_L^4}{(g/\theta) \cdot 4.7} \frac{\partial \bar{\theta}}{\partial z}$$

where the value of the universal constant was taken as 4.7. Assuming that $(g/\theta) = 0.0333$ $m \cdot s^{-2} \cdot K^{-1}$, we find that $\overline{w'\theta'} = 3.4 \times 10^{-3}$ K m/s.

Discussion: Such a small value of heat flux is typical of the upper SBL.

9.5 Neutral Boundary Layer Similarity Relationship Lists

Although boundary layers are rarely exactly neutral, there are situations such as strong winds and overcast skies where the boundary layer is approximately neutral. In a neutral boundary layer the only (or dominant) TKE generation mechanism is mechanical, associated with wind shear and surface stress. Thus, we expect u_* to be important. Rarely is the Obukhov length used, because it is infinite in statically neutral conditions.

Some investigators (Sorbjan, 1986) have suggested similarity parameterizations based on pseudo-local scaling (using scales u_L, θ_L, but including z instead of L_L),while others (Nicholls and Readings, 1979; Grant, 1986) have applied surface-layer similarity relationships higher in the boundary layer (using scales u_*, θ_*, and z,). Occasionally, it is assumed that a well defined top of the turbulent boundary layer can be identified, allowing z_i to be used.

Surface layer parameterizations are often based on the limiting cases of diabatic similarity relationships, for the case where z/L goes to zero (Wyngaard and Coté, 1971; Merry and Panofsky, 1976; Panofsky et al, 1977; Nicholls and Readings, 1979; Smith, 1980; Grant, 1986; and Sorbjan, 1986).

9.5.1 Mean Variables and Their Gradients

Boundary-Layer Parameterizations:

$$\frac{k\,z}{u_L}\frac{\partial \overline{U}}{\partial z} = 1 \qquad (9.5.1a)$$

$$\frac{k\,z}{\theta_L}\frac{\partial \overline{\theta}}{\partial z} = 0.74 \qquad (9.5.1b)$$

Surface-Layer Parameterizations:

$$\frac{k\,z}{u_*}\frac{\partial \overline{U}}{\partial z} = 1 \qquad (9.5.1c)$$

$$\frac{k\,z}{\theta_*^{SL}}\frac{\partial \overline{\theta}}{\partial z} = 0.74 \qquad (9.5.1d)$$

9.5.2 Fluxes (boundary layer)

$$\frac{\left[\overline{u'\theta'}^2 + \overline{v'\theta'}^2\right]^{1/2}}{-\overline{w'\theta'}} = 4 \qquad (9.5.2a)$$

$$\frac{\overline{u'w'}}{\overline{u'w'}_s} = 1 - \frac{z}{z_i} \qquad (9.5.2b)$$

9.5.3 Variances

Boundary-Layer Relationships:

$$\frac{\overline{u'^2} + \overline{v'^2}}{u_L^2} = 8.5 \qquad (9.5.3a)$$

$$\frac{\overline{w'^2}}{u_L^2} = 2.5 \qquad (9.5.3b)$$

$$\frac{\overline{\theta'^2}}{\theta_L^2} = 4 \tag{9.5.3c}$$

$$\frac{\overline{u'^2}}{u_*^2} = 6\left(1 - \frac{z}{z_i}\right)^2 + \frac{z}{z_i}\frac{\overline{u'^2_{top}}}{u_*^2} \tag{9.5.3d}$$

$$\frac{\overline{v'^2}}{u_*^2} = 3\left(1 - \frac{z}{z_i}\right)^2 + \frac{z}{z_i}\frac{\overline{v'^2_{top}}}{u_*^2} \tag{9.5.3e}$$

$$\frac{\overline{w'^2}}{u_*^2} = \left(1 - \frac{z}{z_i}\right)^{1/2} \tag{9.5.3f}$$

Equations (9.5.3 d and e) include an additional ratio for the variance at the top of the boundary layer (assuming a well-defined top) normalized by the surface stress. Although this ratio is expected to vary from situation to situation, during the KONTUR experiment (Grant, 1986) it was found to equal 2.0 for both equations.

Surface-Layer Relationships:

$$\frac{\overline{u'^2}}{u_*^2} = 6.1, \quad 6.2, \quad 6.5 \tag{9.5.3g}$$

$$\frac{\overline{v'^2}}{u_*^2} = 2.9, \quad 3.0, \quad 4.3, \quad 6.1 \tag{9.5.3h}$$

$$\frac{\overline{u'^2} + \overline{v'^2}}{u_*^2} = 8.5 \tag{9.5.3i}$$

$$\frac{\overline{w'^2}}{u_*^2} = 1.0, \quad 1.7, \quad 2.5 \tag{9.5.3j}$$

$$\frac{\overline{\theta'^2}}{\theta_*^{SL\,2}} = 4 \tag{9.5.3k}$$

9.5.4 Miscellaneous

Boundary-Layer Relationships:

$$\frac{k z \varepsilon}{u_L^3} = 1 \tag{9.5.4a}$$

Surface-Layer Relationships:

$$\frac{k z \varepsilon}{u_*^3} = 1 \tag{9.5.4b}$$

$$\frac{k z \varepsilon}{u_*^3} = \left(1 + 0.5 \left| \frac{z}{L} \right|^{2/3} \right)^{3/2} \tag{9.5.4c}$$

$$\frac{\overline{w'e}}{u_*^3} = -2.3 \frac{z}{L} \tag{9.5.4d}$$

These last two relationships are designed for near neutral situations.

9.5.5 Example

Problem: In a neutral surface layer with $u_* = 0.2$ m/s, find the TKE dissipation rate as a function of height.

Solution: Rearranging equation (9.5.4b), we can see that the dissipation rate decreases inversely with height:

$$\varepsilon = \frac{u_*^3}{k z} = \frac{0.04}{z} \text{ m}^2\text{s}^{-3} \quad \text{for } z \text{ in meters.}$$

Discussion: As verified by the TKE budget figures in Chapter 5, the dissipation rate is indeed very large near the ground. However, the equation above suggests that the dissipation rate is infinite at the surface, which is clearly unrealistic.

9.6 Convective Boundary Layer Similarity Relationship Lists

When turbulence in a mixed layer is driven by buoyancy and capped at a well defined height, it is obvious that w_* and z_i are important scales for all variables. In addition, when considering heat, moisture, and momentum fluxes we should include the θ_*^{ML}, q_*^{ML}, and u_*^{ML} scales, respectively. Many investigators have examined the convective mixed layer and unstable surface layer (Businger, et.al., 1971; Lenschow, 1974; Lenschow, et al., 1980; Caughey and Readings, 1974, 1975; Caughey and Palmer, 1979; Kaimal, et al., 1976; Smedman and Högström, 1983; Wyngaard, et.al., 1971; LeMone and Pennell, 1976; Brost, et.al., 1982; Berkowicz and Prahm, 1984; Webb, 1982; Zhou, et.al., 1985; and Sorbjan, 1986).

In the surface layer, local free-convective or Monin-Obukhov similarity can be applied depending on the relative importance of surface heating and stress (Wyngaard, et.al., 1971; Berkowicz and Prahm, 1984; Sorbjan, 1986).

9.6.1 Mean Variables and Their Gradients

Mixed-Layer Relationships:

$$\frac{z_i}{w_*}\frac{\partial \overline{U}}{\partial z} = 0 \qquad \text{for } 0.1\, z_i \le z \le 0.9\, z_i \tag{9.6.1a}$$

$$\frac{z_i}{\theta_*^{ML}}\frac{\partial \overline{\theta}}{\partial z} = 0,\quad 1.4 \qquad \text{for } 0.1\, z_i \le z \le 0.9\, z_i \tag{9.6.1b}$$

$$\frac{z_i}{q_*^{ML}}\frac{\partial \overline{q}}{\partial z} = -5 \qquad \text{for } 0.1\, z_i \le z \le 0.9\, z_i \tag{9.6.1c}$$

Investigators (Mahrt and André, 1983) have become more aware that forcings can occur at the top of the mixed layer that are quasi-independent of the forcings at the ground. Entrainment can introduce fluxes at the top of the mixed layer, and shear across the entrainment zone can generate additional turbulence that does not scale with w_*.

Wyngaard and Brost (1984) and Moeng and Wyngaard (1984) have suggested a conceptual model called ***top down - bottom up*** diffusion, which models the contributions of mixing down from the top of the ML separately from mixing up from the ground. One result of this approach is a similarity relationship for gradients of mean variables within the middle 80% of the ML. The relationship for pollutant concentration is given below, but it can be applied just as easily to temperature, moisture, or wind gradients. More details of this method are discussed in Chapter 11.

$$\frac{\partial \overline{C}}{\partial z} = -0.4 \frac{\overline{w'c'}_s}{w_* z_i} \left(\frac{z}{z_i}\right)^{-3/2} + \frac{\overline{w'c'}_{top}}{w_* z_i} \left(1 - \frac{z}{z_i}\right)^{-3/2} \qquad (9.6.1d)$$

The gradient on the left of the equal sign is not normalized into a dimensionless group, because there is no single pollutant scale. Pollutant fluxes at both the top and bottom of the ML are relevant, and would yield two different pollutant scales.

Surface-Layer Relationships:

$$\phi_M = \frac{k z}{u_*} \frac{\partial \overline{U}}{\partial z} = \left(1 - 15 \frac{z}{L}\right)^{-1/4} \qquad (9.6.1e)$$

$$\phi_H = \frac{k z}{\theta_*^{SL}} \frac{\partial \overline{\theta}}{\partial z} = 0.74 \left(1 - 9 \frac{z}{L}\right)^{-1/2} \qquad (9.6.1f)$$

The above two flux-profile relationships apply when surface stress is nonzero, and have been plotted in Fig 5.24. Alternative relationships that have been proposed for zero stress situations are:

$$\frac{z_i}{w_*} \frac{\partial \overline{U}}{\partial z} = 1.2 \frac{\left[1 - \alpha (z/z_i)\right]^{2/3}}{\left[(z/z_i)^{4/3} (-\mu_i)^{2/3}\right]} \qquad (9.6.1g)$$

$$\frac{z_i}{\theta_*^{ML}} \frac{\partial \overline{\theta}}{\partial z} = \frac{\left[1 - \alpha (z/z_i)\right]^{2/3}}{(z/z_i)^{4/3}} \qquad (9.6.1h)$$

where α is a universal constant in the range 1.2-1.5, and $\mu_i = z_i / L$.

9.6.2 Fluxes for Both the Mixed Layer and Surface Layer

Because the flux profiles are linear with height in the ML, we propose here the following similarity relationships:

$$\frac{\overline{u'w'}}{\overline{u'w'}_s} = 1 - \frac{z}{z_i} + \frac{\overline{u'w'}_{top}}{\overline{u'w'}_s} \frac{z}{z_i} \qquad (9.6.2a)$$

$$\frac{\overline{w'\theta'}}{\overline{w'\theta'}_s} = 1 - \frac{z}{z_i} + \frac{\overline{w'\theta'}_{top}}{\overline{w'\theta'}_s} \frac{z}{z_i} \qquad (9.6.2b)$$

$$\frac{\overline{w'q'}}{\overline{w'q'}_s} = 1 - \frac{z}{z_i} + \frac{\overline{w'q'}_{top}}{\overline{w'q'}_s}\frac{z}{z_i} \qquad (9.6.2c)$$

In the absence of shear or other independent forcings in the entrainment zone, the flux at the top of the mixed layer can be related to the flux at the bottom, resulting in the following simplified similarity relationships:

$$\frac{\overline{w'\theta'}}{\overline{w'\theta'}_s} = 1 - \alpha\frac{z}{z_i} \qquad \text{where } \alpha = 1.2 \text{ to } 1.5 \qquad (9.6.2d)$$

$$\frac{\overline{u'\theta'}}{\overline{w'\theta'}_s} = 0.5\left(1 - 2.2\frac{z}{z_i}\right) \qquad (9.6.2e)$$

9.6.3 Variances

Mixed-Layer Relationships: All of the following expressions fail in and near the entrainment zone at the top of the mixed layer, where locally generated turbulence and buoyancy waves can contribute to the variance.

$$\frac{\overline{u'^2}}{u_{*ML}^2} = \text{constant} \qquad (9.6.3a)$$

$$\frac{\overline{v'^2}}{u_{*ML}^2} = \text{constant} \qquad (9.6.3b)$$

$$\frac{\overline{w'^2}}{w_*^2} = 1.8\left(\frac{z}{z_i}\right)^{2/3}\cdot\left(1 - 0.8\frac{z}{z_i}\right)^2 \qquad (9.6.3c)$$

$$\frac{\overline{\theta'^2}}{\theta_{*ML}^2} = 1.8\left(\frac{z}{z_i}\right)^{-2/3} \qquad (9.6.3d)$$

$$\frac{\overline{q'^2}}{q_*^{ML\,2}} = 1.8 \left(\frac{z}{z_i}\right)^{-2/3} \qquad (9.6.3e)$$

One might expect that relationships similar to (9.5.3 d & e) would work well for the mixed layer, assuming that the variance at the top of the mixed layer could be parameterized. This approach has not been explored in the literature.

Surface-Layer Relationships: When stress is nonzero, the following expressions are appropriate:

$$\frac{\left(\overline{w'^2}\right)^{1/2}}{u_*} = 1.9 \cdot \left(-\frac{z}{L}\right)^{1/3} \qquad (9.6.3f)$$

$$\frac{\left(\overline{\theta'^2}\right)^{1/2}}{\theta_*^{SL}} = -0.95 \cdot \left(-\frac{z}{L}\right)^{-1/3} \qquad (9.6.3g)$$

In cases of local free convection (calm winds) the following expressions are useful:

$$\frac{\overline{\theta'^2}}{\theta_{Lf}^2} = 1.85, \quad 2 \qquad (9.6.3h)$$

$$\frac{\overline{w'^2}}{w_{Lf}^2} = 1.21, \quad 1.6 \qquad (9.6.3i)$$

The following expressions combine mixed layer scaling with local free convection:

$$\frac{\overline{w'^2}}{w_*^{ML2}} = 1.6 \left(\frac{z}{z_i}\right)^{2/3} \left(1 - 1.2\frac{z}{z_i}\right)^{2/3} \qquad (9.6.3j)$$

$$\frac{\overline{\theta'^2}}{\theta_*^{ML2}} = 2\,\frac{(1 - 1.2\,z/z_i)^{4/3}}{(z/z_i)^{2/3}} \qquad (9.6.3k)$$

$$\frac{\overline{\theta'^2}}{\theta_*^{ML2}} = \frac{\overline{q'^2}}{q_*^{ML2}} = 1.8 \left(\frac{z}{z_i}\right)^{-2/3} \tag{9.6.3l}$$

9.6.4 Miscellaneous

Mixed-Layer Relationships:

$$\frac{\overline{w'^3}}{w_*^3} = 0.8 \frac{z}{z_i}\left(1 - \frac{1.1\,z}{z_i}\right) \tag{9.6.4a}$$

$$\frac{\varepsilon z_i}{w_*^3} = \text{constant with height above the surface layer} \tag{9.6.4b}$$

$$\frac{\overline{w'e}}{w_*^3} = 0.8 \frac{z}{z_i}\left(1 - 0.9\frac{z}{z_i}\right)^2 \tag{9.6.4c}$$

$$\frac{z_i\,\overline{w'\theta'}}{w_*\,\theta_*^{ML2}}\left(\frac{\partial\bar{\theta}}{\partial z}\right) = 1.4 - 2\frac{z}{z_i} \tag{9.6.4d}$$

$$\frac{\overline{w'\theta'^2}}{w_*\,\theta_*^{ML2}} = 3.1\left(1 - \frac{z}{z_i}\right)^3 \tag{9.6.4e}$$

$$\frac{\overline{w'^2\,\theta'}}{w_*^2\,\theta_*^{ML}} = 0.5\left(1 - 1.2\frac{z}{z_i}\right) \tag{9.6.4f}$$

$$\frac{z_i\,\overline{w'^2}}{w_*^2\,\theta_*^{ML}}\left(\frac{\partial\bar{\theta}}{\partial z}\right) = 2.5\left(\frac{z}{z_i}\right)^{2/3}\left(1 - 0.8\frac{z}{z_i}\right)^2 \tag{9.6.4g}$$

$$\frac{z_i\,\overline{w'q'}}{w_*\,(q_*^{ML})^2}\left(\frac{\partial\bar{q}}{\partial z}\right) = -5 + 2.5\frac{z}{z_i} \tag{9.6.4h}$$

$$\frac{\overline{w'^2 q'}}{w_*^2 q_*^{ML}} = 0.6\left(1 - 0.4\frac{z}{z_i}\right) \tag{9.6.4i}$$

$$\frac{z_i \overline{w'^2}}{w_*^2 q_*^{ML}}\left(\frac{\partial \bar{q}}{\partial z}\right) = -9\left(\frac{z}{z_i}\right)^{2/3}\left(1 - 2\frac{z}{z_i}\right)^2 \tag{9.6.4j}$$

$$\frac{\overline{\theta' q'}}{\theta_*^{ML} q_*^{ML}} = 1.8\left(\frac{z}{z_i}\right)^{-2/3}\left(1 - 2\frac{z}{z_i}\right) \tag{9.6.4k}$$

This last equation has also been applied to the surface layer.

Surface-Layer Relationships: The first equations apply to surface layers with nonzero stress.

$$\frac{\overline{w'e}}{u_*^3} = -2.3\frac{z}{L} \tag{9.6.4l}$$

$$\frac{\overline{w'^2 \theta'}}{u_*^2 \theta_*^{SL}} = -1.3\left(-\frac{z}{L}\right)^{1/3} \tag{9.6.4m}$$

$$\frac{k z \overline{w'^2}}{u_*^3}\left(\frac{\partial \bar{U}}{\partial z}\right) = 1.2 - 0.5\frac{z}{L} \tag{9.6.4n}$$

$$\frac{k z \overline{w'^2}}{u_*^2 \theta_*^{SL}}\left(\frac{\partial \bar{\theta}}{\partial z}\right) = 0.9 \tag{9.6.4o}$$

The next equations work best when the stress is very small and buoyancy dominates:

$$\frac{\overline{w'^2 \theta'}}{w_*^2 \theta_*^{ML}} = \frac{\overline{w'^2 q'}}{w_*^2 q_*^{ML}} = 0.9\left(\frac{z}{z_i}\right)^{1/3} \tag{9.6.4p}$$

$$\frac{\overline{w' \theta'^2}}{w_* \theta_*^{ML2}} = \left(-\mu_i \frac{z}{z_i}\right)^{-1/3}\left(1 - 1.2\frac{z}{z_i}\right)^{5/3} \tag{9.6.4q}$$

$$\frac{\varepsilon_q \, z_i}{w_* \, q_*^{ML^2}} = 0.43 \left(\frac{z}{z_i} \right)^{-4/3} \qquad (9.6.4r)$$

9.6.5 Example

Problem: Use similarity theory to develop an expression for vertical velocity variance, $\overline{w'^2}$, as a function of height given the (synthetic) measurements in Table 9-2.

Table 9-2. Synthetic vertical velocity variance data.

z (m)	$\overline{w'^2}$ (m^2s^{-2}) Day 1	Day 2	Day 3	Day 4
1500				0.4
1400				0.6
1300				0.8
1200				1.0
1100				1.1
1000		0.10		1.3
900		0.16		1.4
800		0.22		1.4
700	0.6	0.30		1.5
600	0.9	0.37		1.6
500	1.2	0.39		1.6
400	1.5	0.40		1.5
300	1.6	0.40	0.20	1.4
200	1.5	0.36	0.36	1.2
100	1.2	0.28	0.40	1.0
0	0.8	0.20	0.20	0.8
z_i (m)	750	1000	350	1500
$\overline{w'\theta_{v_s}'}$ (K m/s)	0.33	0.03	0.09	0.16

Solution: Although this data set exhibits a variety of magnitudes over a range of heights, each of the individual data curves has the same shape (see Fig 9.3a) — a clue that they are created by a common physical process that could possibly be described empirically.

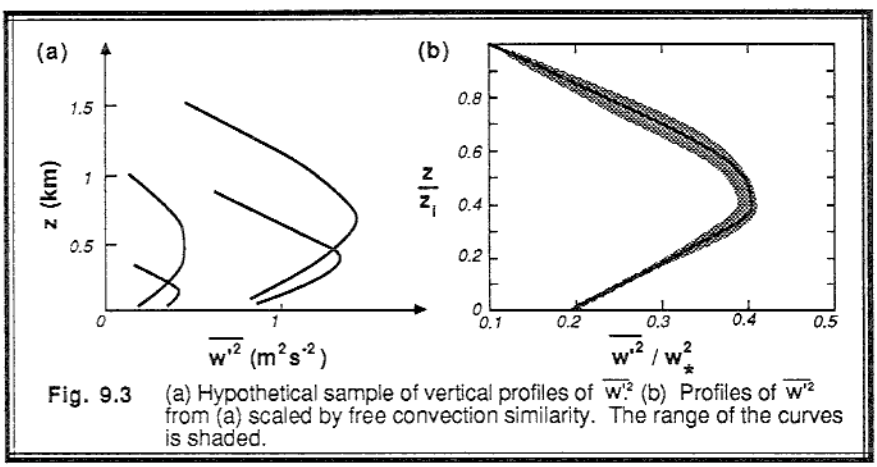

Fig. 9.3 (a) Hypothetical sample of vertical profiles of $\overline{w'^2}$ (b) Profiles of $\overline{w'^2}$ from (a) scaled by free convection similarity. The range of the curves is shaded.

The tabulated data includes mixed layer depth and surface heat flux. From these, we can calculate the length and velocity scales, z_i and w_*, assuming $g/\overline{\theta_v} = 0.0333\ ms^{-2}K^{-1}$. Using Buckingham Pi analysis, or by inspection for this simple case, we can create the following dimensionless groups: z/z_i, and $\overline{w'^2}/w_*^2$. When the original data is replotted in this dimensionless framework, lo and behold most of the data points collapse into a single curve, as plotted in Fig 9.3b. Thus, all of the data are similar, allowing us to use similarity theory.

By trial and error using simply power laws, we find that the following equation approximates the shape of the data, and is plotted as the curve in Fig 9.3b:

$$\frac{\overline{w'^2}}{w_*^2} = 1.7 \left(\frac{z}{z_i}\right)^{2/3} \cdot \left(1 - 0.8\,\frac{z}{z_i}\right)^2$$

This equation is almost identical to (9.6.3c), except for the value of the regression coefficient (i.e., 1.7 vs. 1.8).

Discussion: The hope is that this equation, and the corresponding curve in Fig 9.3b, are "universal"; that is, they should work just as well for other free convection

situations. For example, on a different day with $z_i = 1200$ m and $\overline{w'\theta_v'}_s = 0.2$ K m/s, we might wish to know the vertical velocity variance at z = 500 m without performing an experiment to measure it ourselves. At that height, $z/z_i = 0.42$, which can be used in the above equation or with Fig 9.3b directly to give us $\overline{w'^2}/w_*^2 = 0.42$. Since $w_* = 2$ m/s based on flux and z_i data given at the start of this example, we can easily solve for $\overline{w'^2} = 1.68$ $m^2 s^{-2}$.

The above example was more than just a contrived didactic case. If you look back at Fig 4.2a, you will see that vertical velocity variance measurements do indeed vary with height as described here.

9.7 The Log Wind Profile

One important application of similarity theory is to the mean wind profile in the surface layer. Since people spend most of their lives within the surface layer, the variation of wind speed with height affects their daily lives. The nature of this profile dictates the structure of buildings, bridges, snow fences, wind breaks, pollutant dispersion, and wind turbines, for example. Also, the surface layer wind profile has been studied extensively because of its accessibility to surface-based measurements.

As shown in Fig 9.4, the wind speed usually varies approximately logarithmically with height in the surface layer. Frictional drag causes the wind speed to become zero close to the ground, while the pressure gradient forces cause the wind to increase with height.

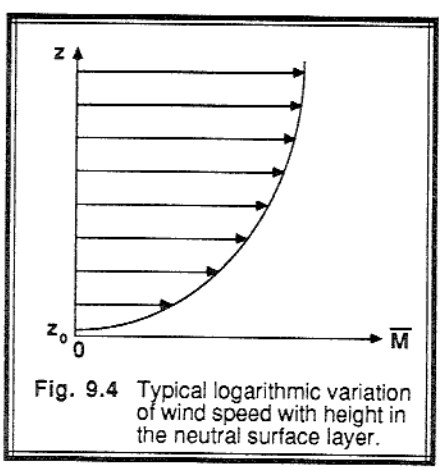

Fig. 9.4 Typical logarithmic variation of wind speed with height in the neutral surface layer.

When plotted on semi-log graph paper (Fig 9.5), a logarithmic relationship such as the wind profile in statically neutral situations appears as a straight line. For non-neutral situations, the wind profile deviates slightly from logarithmic. In stable boundary layers, the wind profile is concave downward on a semi-log plot, while unstable boundary layers are concave upward (see Fig 9.5).

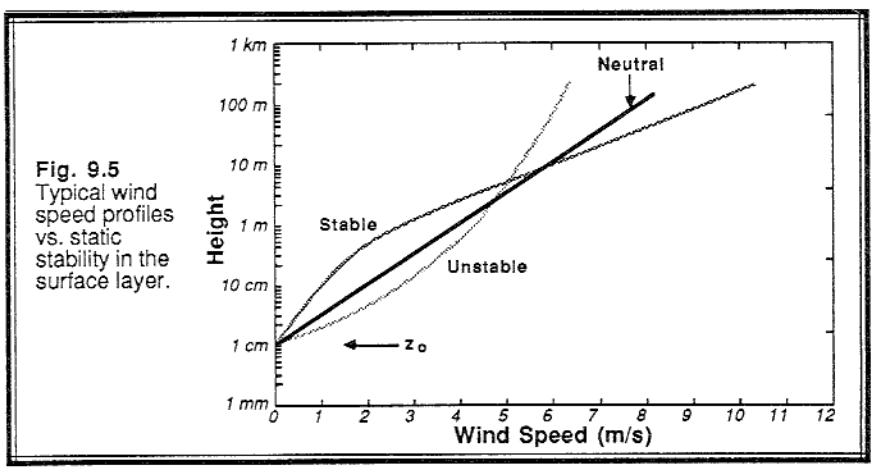

Fig. 9.5 Typical wind speed profiles vs. static stability in the surface layer.

9.7.1 Wind Profile in Statically Neutral Conditions

To estimate the mean wind speed, $\overline{M}$, as a function of height, z, above the ground, we speculate that the following variables are relevant: surface stress (represented by the friction velocity, u_*), and surface roughness (represented by the ***aerodynamic roughness length***, z_o). Upon applying Buckingham Pi Theory, we find the following two dimensionless groups: $\overline{M}/u_*$, and z/z_o. Based on the data already plotted in Figs 9.4 and 9.5, we might expect a logarithmic relationship between these two groups:

$$\frac{\overline{M}}{u_*} = \left(\frac{1}{k}\right) \ln\left(\frac{z}{z_o}\right) \qquad (9.7.1a)$$

where (1/k) is a constant of proportionality. As discussed before, the von Karman constant, k, is supposedly a universal constant that is not a function of the flow nor of the surface. The precise value of this constant has yet to be agreed on, but most investigators feel that it is either near k = 0.35 or k = 0.4.

For simplicity, meteorologists often pick a coordinate system aligned with the mean wind direction near the surface, leaving $\overline{V} = 0$ and $\overline{U} = \overline{M}$. This gives the form of the log wind profile most often seen in the literature:

$$\overline{U} = \left(\frac{u_*}{k}\right) \ln\left(\frac{z}{z_o}\right) \qquad (9.7.1b)$$

An alternative derivation of the log wind profile is possible using mixing length theory. Recall from Chapter 6 that the momentum flux in the surface layer is: $\overline{u'w'} = -k^2 z^2 |\partial\overline{U}/\partial z| \partial\overline{U}/\partial z$. But since the momentum flux is approximately constant with height in the surface layer, $\overline{u'w'}(z) = \overline{u'w'}(z=0) = u_*^2$. Substituting this into the mixing length expression and taking the square root of the whole equation gives

$$\frac{\partial\overline{M}}{\partial z} = \frac{u_*}{k\,z} \qquad (9.7.1c)$$

When this is integrated over height from $z = z_o$ (where $\overline{M}=0$) to any height z, we again arrive at (9.7.1b). This derivation is more sound than that of Buckingham Pi, because it predicts a log wind profile theoretically, without resorting to empirical arguments.

If we divide both sides of (9.7.1c) by $[u_*/(kz)]$, we find that the ***dimensionless wind shear*** (ϕ_M , see Chapter 5 or Appendix A) is equal to unity in the neutral surface layer:

$$\phi_M = \left(\frac{k\,z}{u_*}\right)\frac{\partial\overline{M}}{\partial z} = 1 \qquad (9.7.1d)$$

This result was previously listed as (9.5.1c). Equations (9.4.1c) and (9.6.1e) also approach the above expression in the neutral limit of (z/L) approaching zero. In essence, each of these equations describes a log wind profile.

9.7.2 Aerodynamic Roughness Length

The aerodynamic roughness length, z_o, is defined as the height where the wind speed becomes zero. The word ***aerodynamic*** comes about because the only true determination of this parameter is from measurements of the wind speed at various heights. Given observations of wind speed at two or more heights, it is easy to solve for z_o and u_* . Graphically, we can easily find z_o by extrapolating the straight line drawn through the wind speed measurements on a semi-log graph (see Fig 9.5) to the height where $\overline{M} = 0$ (i.e., extrapolate the line towards the ordinate axis).

Although this roughness length is NOT equal to the height of the individual ***roughness elements*** on the ground, there IS a one-to-one correspondence between those roughness elements and the aerodynamic roughness length. In other words, once the aerodynamic roughness length is determined for a particular surface, it does not change with wind speed, stability, or stress. It can change if the roughness elements on the surface change, such as caused by changes in the height and coverage of vegetation, erection of fences, construction of houses, deforestation or lumbering, etc.

Typical values of the roughness length are indicated in Fig 9.6 (Smedman-Högström & Högström, 1978; Hicks, et al, 1975; Garratt, 1977; Nappo, 1977; Thompson, 1978; and Kondo and Yamazawa, 1986). As expected, higher roughness elements are associated with larger aerodynamic roughness lengths. In all cases, however, the aerodynamic roughness length is smaller than the physical height of the roughness element.

Lettau (1969) suggested a method for estimating the aerodynamic roughness length based on the average vertical extent of the roughness elements (h*), the average silhouette or vertical cross-section area presented to the wind by one element (s_s), and the lot size per element [S_L = (total ground surface area / number of elements)]

$$z_o = 0.5\, h^* \left(\frac{s_s}{S_L} \right) \tag{9.7.2a}$$

This relationship is acceptable when the roughness elements are evenly spaced, not too close together, and of similar height and shape.

Kondo and Yamazawa (1986) proposed a similar relationship, where variations in individual roughness elements were accounted for. Let s_i represent the actual horizontal surface area occupied by element i, and h_i be the height of that element. If N elements occupy a total area of S_T, then the roughness length can be approximated by:

$$z_o = \frac{0.25}{S_T} \sum_{i=1}^{N} h_i\, s_i \quad = \frac{0.25}{L_T} \sum_{i=1}^{N} h_i\, w_i \tag{9.7.2b}$$

An approximation of the aerodynamic roughness can also be made by summing over the individual roughness elements encountered while traveling along a straight line of total length L_T. For this case, one must consider the longitudinal width, w_i, of each element in the direction of travel. These expressions have been applied successfully to buildings in cities.

We have already discussed Charnock's relationship for the roughness length of the sea surface, which can also be applied to blowing sand and blowing snow (Chamberlain, 1983) with appropriate change in parameter, α_c:

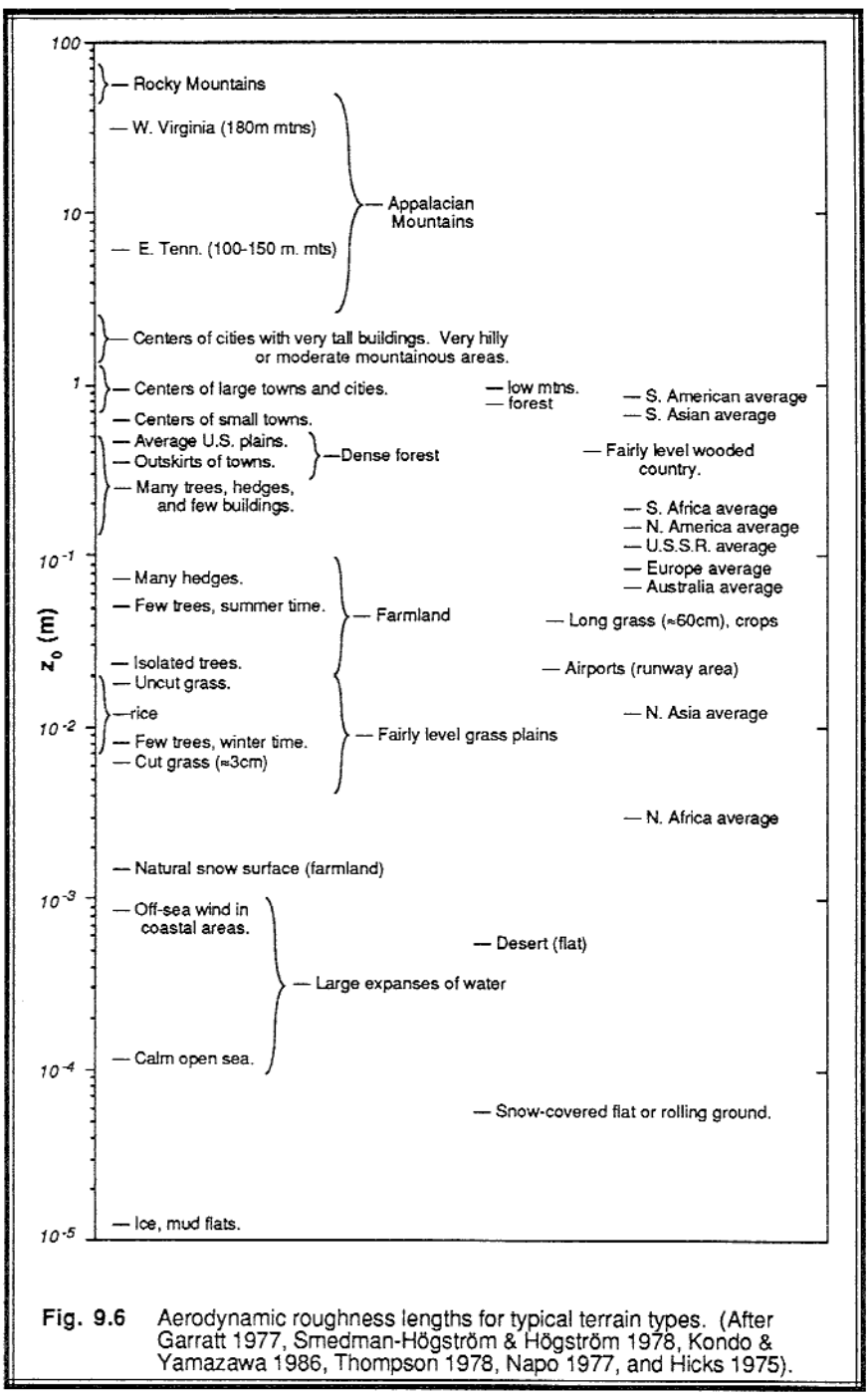

Fig. 9.6 Aerodynamic roughness lengths for typical terrain types. (After Garratt 1977, Smedman-Högström & Högström 1978, Kondo & Yamazawa 1986, Thompson 1978, Napo 1977, and Hicks 1975).

$$z_o = \frac{\alpha_c u_*^2}{g} \qquad (9.7.2c)$$

For the sea, $\alpha_c = 0.016$.

For many large-scale numerical weather-forecast models the lowest grid-points (at height z_1 above the surface) are so high that the surface layer is not resolved. Nevertheless, it is important to account for varying roughness in the model forecast. André and Blondin (1986) suggested that the ***effective roughness length*** ($z_{o_{eff}}$) to be used in the model decreases as the altitude of the lowest grid point increases. In particular, the ratio $(z_{o_{eff}})/h^*$ decreases from about 0.1 to 0.01 as z_1 increases from 0.1 km to 1 km. Taylor (1987), however, suggests that $z_{o_{eff}}$ is independent of z_1.

9.7.3 Displacement Distance

Over land, if the individual roughness elements are packed very closely together, then the top of those elements begins to act like a displaced surface. For example, in some forest canopies the trees are close enough together to make a solid-looking mass of leaves, when viewed from the air. In some cities the houses are packed close enough together to give a similar effect; namely, the average roof-top level begins to act on the flow like a displaced surface.

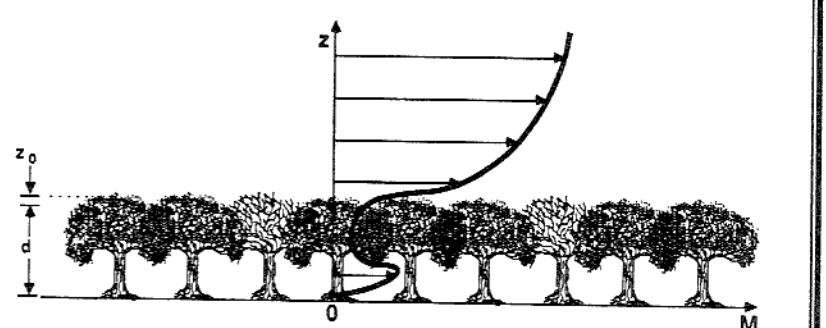

Fig. 9.7 Flow over forest canopy showing wind speed, M, as a function of height, z. The thick canopy layer acts like a surface displaced a distance, d, above the true surface. z_0 = roughness length.

Above the canopy top, the wind profile increases logarithmically with height, as shown in Fig 9.7. Thus, we can define both a displacement distance, d, and a roughness length, z_o, such that:

$$\overline{M} = \left(\frac{u_*}{k}\right) \ln\left[\frac{(z - d)}{z_o}\right] \qquad (9.7.3a)$$

for statically neutral conditions, where we now define $\overline{M} = 0$ at $z = d + z_o$. Given wind speed observations in statically neutral conditions at three or more heights, it is easy to use computerized non-linear regression algorithms such as the Marquardt Method or the Gauss-Newton Method to solve for the three parameters, u_*, z_o, and d.

If you are unsure whether a nonzero displacement distance is appropriate to your situation, one approach is to plot $\overline{M}$ vs. (z-d) for neutral conditions on a semi-log graph as shown in Fig 9.8. As a first guess, try d = 0. If your selected d is too small, then the plotted profile will curve concave upward. Use the intercept of this curve on the ordinate to provide the next guess for d. If d is too large, then the curve will be concave downward. Iterate until the plotted data shows no curvature. This trick will not work for non-neutral cases, nor for profiles that cross through internal boundary layers.

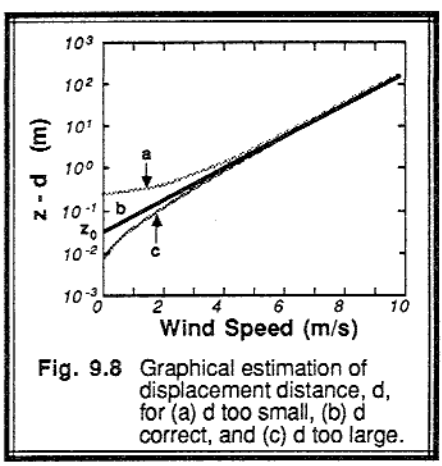

Fig. 9.8 Graphical estimation of displacement distance, d, for (a) d too small, (b) d correct, and (c) d too large.

Finally, if one knows the wind speed at three heights, then the following algebraic expression is easy to derive for the displacement distance.

$$\frac{(\overline{M}_2 - \overline{M}_1)}{(\overline{M}_3 - \overline{M}_1)} \ln\left(\frac{z_3 - d}{z_1 - d}\right) = \ln\left(\frac{z_2 - d}{z_1 - d}\right) \qquad (9.7.3b)$$

The disadvantage of this expression is that it is not explicit in d. However, this equation can be iteratively solved for d.

9.7.4 Surface Stress

In Fig 9.5, u_* is proportional to the slope of the line, in statically neutral conditions. In fact, once the roughness length and displacement distance have been determined, it is easy to find the u_* from:

$$u_* = \frac{k\,\overline{M}}{\ln (z/z_o)} \tag{9.7.4}$$

where $\overline{M}$ is the wind speed at height z. The magnitude of the surface stress in kinematic form is then u_*^2.

9.7.5 Wind Profile in Non-neutral Conditions

Expressions such as (9.7.1b) or (9.7.1d) for statically neutral flow relate the momentum flux, as described by u_*^2, to the vertical profile of $\overline{U}$-velocity. Hence, those expressions can be called ***flux-profile relationships***. These relationships can be extended to include non-neutral (***diabatic***) surface layers.

Businger-Dyer Relationships. In non-neutral conditions, we might expect that the buoyancy parameter and the surface heat flux are additional relevant variables. When these are used with the variables from Section 9.7.1, Buckingham Pi analysis gives us three dimensionless groups (neglecting the displacement distance for now): $\overline{M}/u_*$, z/z_o, and z/L, where L is the Obukhov length. Alternatively, if we consider the shear instead of the speed, we get two dimensionless groups: ϕ_M and z/L. Based on field experiment data, Businger, et al., (1971) and Dyer (1974) independently estimated the functional form to be:

$$= 1 + \left(\frac{4.7\,z}{L}\right) \qquad \text{for } \frac{z}{L} > 0 \quad \text{(stable)} \tag{9.7.5a}$$

$$\phi_M = 1 \qquad \text{for } \frac{z}{L} = 0 \quad \text{(neutral)} \tag{9.7.5b}$$

$$= \left[1 - \left(\frac{15z}{L}\right)\right]^{-1/4} \qquad \text{for } \frac{z}{L} < 0 \quad \text{(unstable)} \tag{9.7.5c}$$

These are plotted in Fig 9.9a, where Businger, et al., have suggested that k = 0.35 for their data set.

Similar expressions have been estimated for the heat flux vs. the virtual potential temperature profile:

$$= \frac{K_m}{K_H} + \frac{4.7\,z}{L} \qquad \text{for } \frac{z}{L} > 0 \text{ (stable)} \qquad (9.7.5d)$$

$$\phi_H = \frac{K_m}{K_H} \qquad \text{for } \frac{z}{L} = 0 \text{ (neutral)} \qquad (9.7.5e)$$

$$= \frac{K_m}{K_H}\left[1 - \frac{9\,z}{L}\right]^{-1/4} \qquad \text{for } \frac{z}{L} < 0 \text{ (unstable)} \qquad (9.7.5f)$$

where (K_m / K_H) is the ratio of eddy diffusivities of heat and momentum. This ratio equals 0.74 in neutral conditions. The curves corresponding to the above equations are plotted in Fig 9.9b. It is often assumed that the flux profile relationships for moisture or pollutants are equal to those for heat.

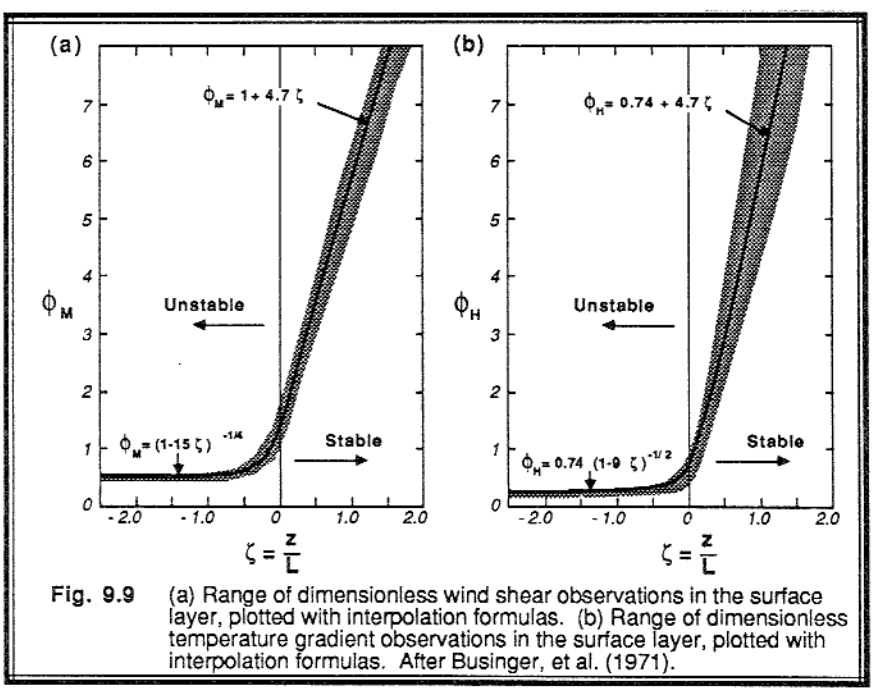

Fig. 9.9 (a) Range of dimensionless wind shear observations in the surface layer, plotted with interpolation formulas. (b) Range of dimensionless temperature gradient observations in the surface layer, plotted with interpolation formulas. After Businger, et al. (1971).

Diabatic Wind Profile. The Businger-Dyer relationships can be integrated with height to yield the wind speed profiles:

$$\frac{\overline{M}}{u_*} = \left(\frac{1}{k}\right)\left[\ln\left(\frac{z}{z_o}\right) + \Psi_M\left(\frac{z}{L}\right)\right] \qquad (9.7.5g)$$

where the function $\Psi(z/L)$ is given for stable conditions ($z/L > 0$) by:

$$\Psi_M\left(\frac{z}{L}\right) = \frac{4.7\ z}{L} \qquad (9.7.5h)$$

and for unstable ($z/L < 0$) by:

$$\Psi_M\left(\frac{z}{L}\right) = -2\ln\left[\frac{(1+x)}{2}\right] - \ln\left[\frac{(1+x^2)}{2}\right] + 2\tan^{-1}(x) - \frac{\pi}{2} \qquad (9.7.5i)$$

where $x = [1 - (15z/L)]^{1/4}$. This last equation was presented by Paulson (1970), although alternative expressions that are more easily solved on computer were presented by Nickerson and Smiley (1975) and Benoit (1977). In the limit of statically neutral flow ($z/L = 0$), both of these relationships reduce to the log wind profile.

When (9.7.5g and h) are combined, the resulting equation describes a ***log-linear profile,*** because $\overline{M}$ depends on both ln(z) and linearly on z/L. As plotted in Fig 9.5, the linear term causes the winds in the surface layer to increase with height faster than those of a neutral profile. This feature is expected on the underside of the nocturnal jet. Clearly the equation fails near the top of the nocturnal boundary layer, where the wind speed reaches a maximum and then frequently decreases with height. Thus, we must be content with applying the log-linear profile only within the stable surface layer.

Fluxes and Scaling Parameters. If the stability and the flux or stress is known in advance, then the integrated Businger-Dyer relationships can be solved directly for the wind speed or the potential temperature at any height.

Often, these equations are used in reverse, to estimate the flux knowing the mean wind or temperature profile. This is much more difficult. For example, u_*, appears in a number of places in the right hand side of (9.7.5g-i): once explicitly, and additional times hidden in L. Furthermore, L is a function of the heat flux, which must simultaneously be estimated from the temperature profile. The resulting coupled set of equations is very difficult to solve, and often involves an iterative approach. One way around this problem is to simplify the flux profile relationships.

For statically unstable conditions, Businger, et.al. (1971) found:

$$\frac{z}{L} = Ri, \tag{9.7.5j}$$

where Ri is the gradient Richardson number (see Fig 5.23 of Chapt. 5). Since Ri is based on gradients of mean potential temperature and wind, it is easy to calculate directly from measurements of those mean variables. Thus, the calculation of the u_* or θ_*^{SL} in (9.7.5i) is much easier.

For statically stable conditions, Arya (1981) suggested that the shape similarity of the temperature and wind profiles be utilized, to yield $u_*/\theta_*^{SL} = \Delta\overline{M}/\Delta\overline{\theta}$, where the differences Δ are taken vertically within the surface layer. These simplifications lead to:

$$L \cong \frac{u_* \overline{\theta}\, \Delta\overline{M}}{(k\, g\, \Delta\overline{\theta})} \tag{9.7.5k}$$

where

$$u_* \cong \frac{\left[k\overline{M} - \left\{ \frac{4.7\, k\, g\, \Delta\overline{\theta}\, z}{(\overline{\theta}\, \Delta\overline{M})} \right\} \right]}{\ln\left(\frac{z}{z_o}\right)} \tag{9.7.5l}$$

9.8 Rossby-number Similarity and Profile Matching

As introduced earlier, it is often necessary to be able to approximate the surface stress and fluxes in terms of mean variables at the grid points in numerical models. Unfortunately, in some models the lowest grid point is well above the surface layer, making it impossible to use the flux-profile relationships described earlier. By matching surface layer profiles to flows in the mid-boundary layer, surface fluxes can be related to conditions higher in the boundary layer.

The ***profile matching*** technique uses two separate similarity approximations: one that describes the departure of the actual wind from geostrophic (i.e., the ***geostrophic departure***) in the (outer) mid-boundary layer:

$$\frac{(\overline{M} - M_2)}{u_*} = \left(\frac{1}{k}\right) A\left(\frac{z}{h_2}, \frac{h_2}{L}\right)$$

and the other for the log profile lower in the (inner) surface layer:

$$\frac{\overline{M}}{u_*} = \left(\frac{1}{k}\right)\left[\ln\left(\frac{h_2}{z_o}\right) + \Psi_M\left(\frac{z}{L}\right)\right]$$

where $A(z/h_2 , h_2/L)$ is some universal function to be determined empirically, and $\overline{M}_2$ and h_2 are velocity and height scales in the outer layer. The flow at the bottom of the mid-boundary layer is matched or fitted to agree with that at the top of the surface layer. The resulting relationship relates the surface stress to the mean flow higher in the interior of the boundary layer.

When this procedure is also performed for heat and moisture, we arrive at the following set of equations:

$$\frac{U_2}{u_*} = \left(\frac{1}{k}\right)\left[\ln\left(\frac{h_2}{z_o}\right) - A\left(\frac{h_2}{L}\right)\right]$$

$$\frac{V_2}{u_*} = -\left(\frac{1}{k}\right) B\left(\frac{h_2}{L}\right) \text{ sign } (f_c)$$

$$\frac{\Delta\theta_s}{\theta_*} = \left[\frac{K_m}{(k\, K_H)}\right]\left[\ln\left(\frac{h_2}{z_o}\right) - C\left(\frac{h_2}{L}\right)\right]$$

$$\frac{\Delta q_s}{q_*} = \left[\frac{K_m}{(k\, K_H)}\right]\left[\ln\left(\frac{h_2}{z_o}\right) - D\left(\frac{h_2}{L}\right)\right] \qquad (9.8a)$$

where A, B, C and D are "universal" functions, and $[K_m/(k\, K_H)] \cong 2$. Yamada (1976) tested a number of velocity scales, and found that $U_2 = \langle\overline{U_g}\rangle$, $V_2 = \langle\overline{V_g}\rangle$ worked best. The length scale, h_2, was best modeled using z_i during the day, and the depth of the turbulent layer at night. With these scales, his analysis of field experiment data yielded the functional forms for A, B and C plotted in Fig 9.10.

These equations can be combined and solved to give the bulk transfer (or drag) coefficients, which allow us to find the surface flux given knowledge of mean variables aloft and at the surface:

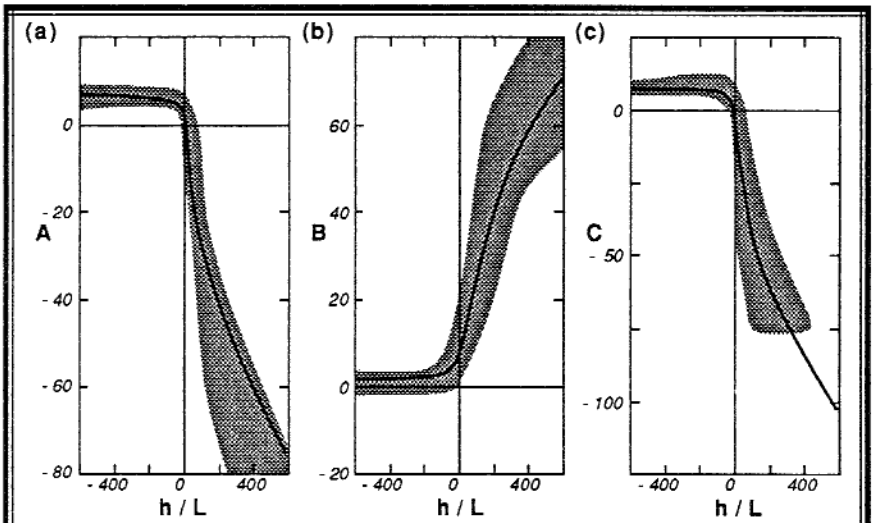

Fig. 9.10 A determination of the "universal" similarity functions vs. h/L based on Wangara field experiment. (a) Similarity function A. (b) B. (c) C. Shaded areas indicate data range, while solid lines are based on equations in the text body. (After Yamada, 1976).

$$C_D = k^2 \left\{ \left[\ln\left(\frac{h_2}{z_o}\right) - A(R_B) \right]^2 + B^2 \right\}^{-1}$$

$$\alpha_{ws} = -\frac{B \cdot (R_B)\, \text{sign}\,(f_c)}{\left[\ln\left(\frac{h_2}{z_o}\right) - A(R_B) \right]}$$

$$C_H = \left[\frac{k\,K_H}{K_m}\right] \left[\ln\left(\frac{h_2}{z_o}\right) - C(R_B) \right]^{-1}$$

$$C_E = \left[\frac{k\,K_H}{K_m}\right] \left[\ln\left(\frac{h_2}{z_o}\right) - D(R_B) \right]^{-1} \qquad (9.8b)$$

where α_{ws} is the angle between the scale-wind direction and the surface stress, $R_B = g\, h_2\, \Delta\theta_s / (\theta\, \overline{M}^2)$ is the bulk Richardson number, and $\Delta\theta_s$ is the temperature difference between the air and the ground (see Table 9-1). Figs 9.11 shows the resulting bulk transfer coefficients for momentum and heat. Because geostrophic wind has proved to be the best scale velocity in these expressions, the equations above are also known as ***geostrophic drag laws.***

Although it is a worthwhile goal to estimate surface flux based on measurements of mean variables aloft, estimates of the universal functions and the bulk transfer coefficients have yielded much scatter. The "universality" of the functions are thus still in question, making this matching scheme of dubious reliability.

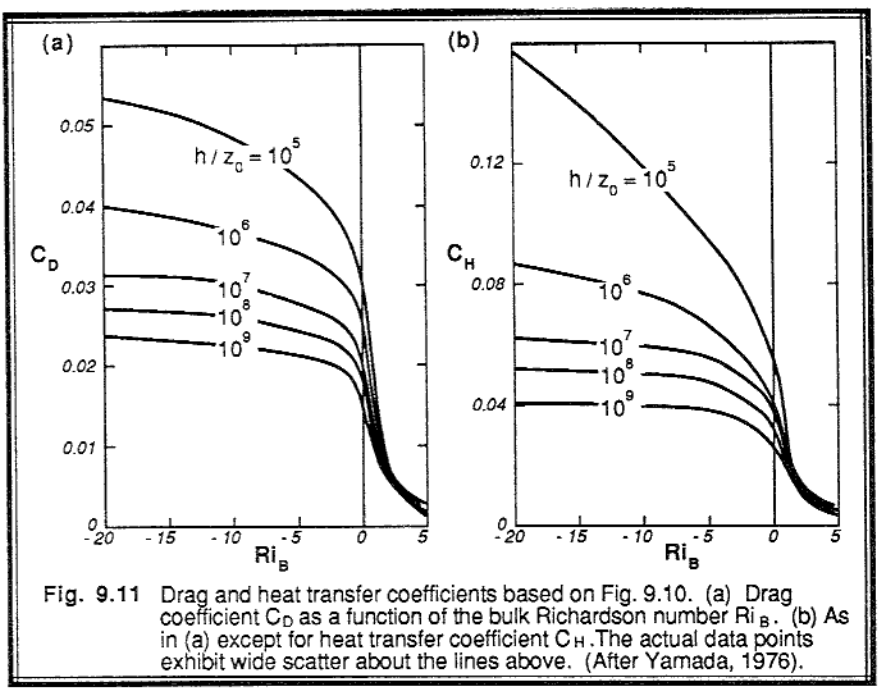

Fig. 9.11 Drag and heat transfer coefficients based on Fig. 9.10. (a) Drag coefficient C_D as a function of the bulk Richardson number Ri_B. (b) As in (a) except for heat transfer coefficient C_H. The actual data points exhibit wide scatter about the lines above. (After Yamada, 1976).

9.9 Spectral Similarity

Spectral analysis of atmospheric turbulence data is a powerful tool to help probe deeper into the workings of turbulent flow. Interest in this method has always been high, as indicated by an issue of Radio Science (1969) dedicated to the spectra of meteorological variables. Nevertheless, there are some fundamental questions regarding the correspondence of Fourier modes to physical eddies (Tennekes, 1976). Similarity theory

has been applied to spectra to help organize the spectral results, and to help focus our understanding about turbulence.

As discussed in the previous chapter, the discrete power spectral intensity measures how much of the variance of a signal is associated with a particular frequency, f. If ξ represents any variable, then the discrete power spectral intensity $E_\xi(f)$ has units of ξ^2. An obvious way to make the spectral intensity dimensionless is to divide it by the total variance $\overline{\xi'^2}$. A continuous spectrum with power spectral density of $S_\xi(f)$ has the same units as ξ^2/f, and can be made dimensionless by dividing by $\overline{\xi'^2}/f$. Analogous expressions can be made for wavenumber spectra instead of frequency spectra. In both of these cases, the result is a spectrum that gives the fraction of total variance explained by a wavelength or wavelength band.

Alternately, if the turbulence is driven or governed by specific mechanisms, such as wind shear, buoyancy, or dissipation, then the spectral intensities can be normalized by scaling variables appropriate to the flow. The next three Sections show normalized spectra for the inertial subrange, for surface layer turbulence generated mechanically, and for mixed layer turbulence generated buoyantly.

9.9.1 Inertial Subrange

As discussed in Chapter 5, there are many situations where middle size turbulent eddies "feel" neither the effects of viscosity, nor the generation of TKE. These eddies get their energy inertially from the larger-size eddies, and lose their energy the same way to smaller-size eddies. For a steady-state turbulent flow, the cascade rate of energy down the spectrum must balance the dissipation rate at the smallest eddy sizes. Hence, there are only three variables relevant to the flow: S, κ, and ε. This similarity approach was pioneered by Kolmogorov (1941) and Obukhov (1941).

By performing a Buckingham Pi dimensional analysis, we can make only one dimensionless group from these three variables:

$$\pi_1 = \frac{S^3 \kappa^5}{\varepsilon^2}$$

We know that this Pi group must be equal to a constant, because there are no other Pi groups for it to be a function of.

Solving the above equation for S yields:

$$S(\kappa) = \alpha_k \varepsilon^{2/3} \kappa^{-5/3} \qquad (9.9.1)$$

where the α_k is known as the ***Kolmogorov constant***. The value of this constant has yet to be pinned down (Gossard, et.al., 1982), but it is in the range of $\alpha_k = 1.53$ to 1.68.

One of the easiest ways to determine whether any measured spectrum has an inertial subrange is to plot the spectrum (S vs. κ) on a log-log graph. The inertial subrange portion should appear as a straight line with a -5/3 slope (see Fig 9.12). The demonstration spectra plotted in Fig 8.9 all have an inertial subrange at normalized frequencies greater than 2.5, assuming that Taylor's hypothesis can be used to relate frequencies to wavenumbers via $f = \overline{M} \cdot \kappa$.

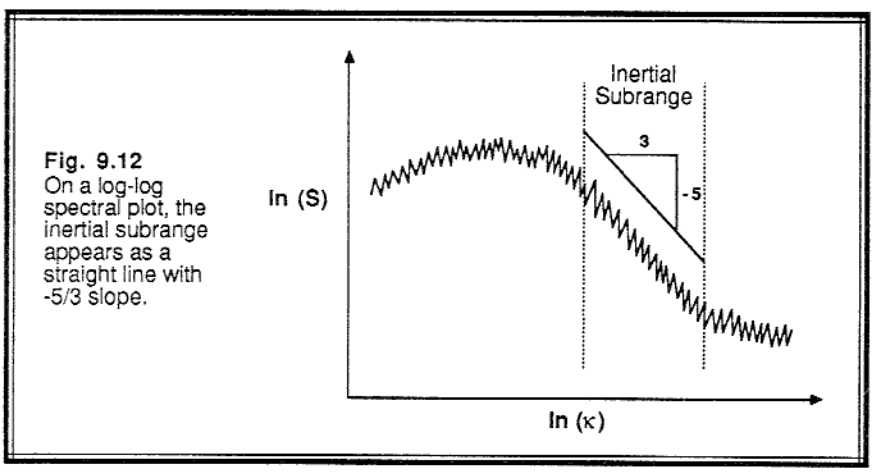

Fig. 9.12 On a log-log spectral plot, the inertial subrange appears as a straight line with -5/3 slope.

9.9.2 Surface Layer Spectra

Suppose that the velocity spectra $fS_u(f)$ for a surface layer in a state of forced convection were likely to be affected by the following variables: u_*, $\overline{w'\theta_v'}_s$, z, $\overline{U}$ (or $\overline{M}$), f, and ε. Buckingham Pi analysis of the above variables gives three dimensionless groups: $\pi_1 = f\, S_u(f) / (k\, z\, \varepsilon)^{2/3}$, $\pi_2 = f\, z / \overline{M}$, and $\pi_3 = z / L$.

Fig 9.13a shows the result when these π groups are plotted (Kaimal, et al, 1972). We see some important characteristics: (1) The peak spectral intensity is reduced as the static stability is increased, because stability is opposing turbulent motions. (2) The peak is shifted to higher frequencies as stability is increased, possibly because the lower frequencies are more strongly damped by the buoyancy forces. (3) At high frequencies, the spectral intensity is no longer dependent on the static stability (at least for the weak stabilities plotted), suggesting that the smaller size eddies in the inertial subrange receive all of their energy via the cascade process from larger eddies, with no direct interaction with the mean flow or the mean stratification. (4) Finally, there is a curious occurrence of an ***excluded region*** in the spectral plot near neutral stratification (lightly shaded in the figure).

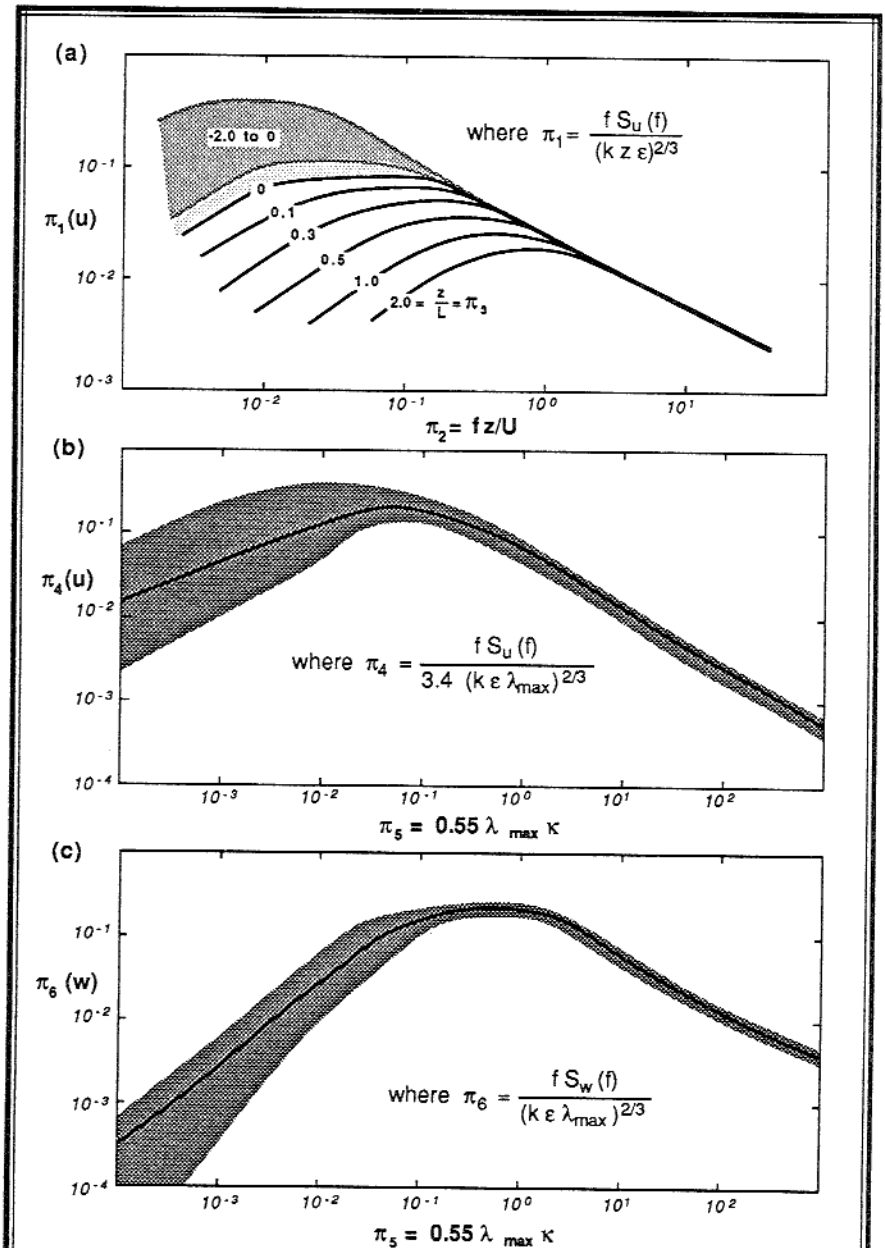

Fig. 9.13 Surface layer spectra scaled by similarity theory for (a) u. When normalized by the wavelength of the spectral peak, λ_{max}, the curves collapse into one curve (b) with some scatter (shaded). Similar results are found for (c) w. (After Kaimal, et al.,1972; and Busch, 1973).

Remember that the correct scaling variables are not specified from first principles, but must be determined from empirical data. For some cases u_*^2 might work, while for other cases $(kz\varepsilon)^{2/3}$ might be better. In a surface layer with turbulence generated mechanically, velocity spectral intensities can be normalized with respect to u_*^2, temperature spectra with respect to $\theta_*^{SL^2}$, and moisture spectra with respect to $q_*^{SL^2}$. Frequency can be normalized by $\overline{M}/z$, $u*/z$, or by frequency, f_{max}, or wavelength, λ_{max}, corresponding to the peak in the spectrum.

When these various spectra are normalized with respect to λ_{max}, all of the curves collapse onto one curve, as shown in Fig 9.13b, where $\pi_4 = f \cdot S_u(f)/[3.4\ (k\ \varepsilon\ \lambda_{max})^{2/3}]$, $f = \kappa\ \overline{M}$, and $\pi_5 = 0.55\ \lambda_{max}\ k$. A similar result is found for vertical velocity spectra (Fig 9.13c), where $\pi_6 = f \cdot S_w(f)/[(k\ \varepsilon\ \lambda_{max})^{2/3}]$.

9.9.3 Mixed Layer Spectra

We might speculate that the following variables affect the velocity spectrum, $fS_u(f)$, during convective conditions: $(g/\overline{\theta_v})\overline{w'\theta_v'}_s$, f, z, z_i, $\overline{U}$ (or $\overline{M}$), and ε. Buckingham Pi

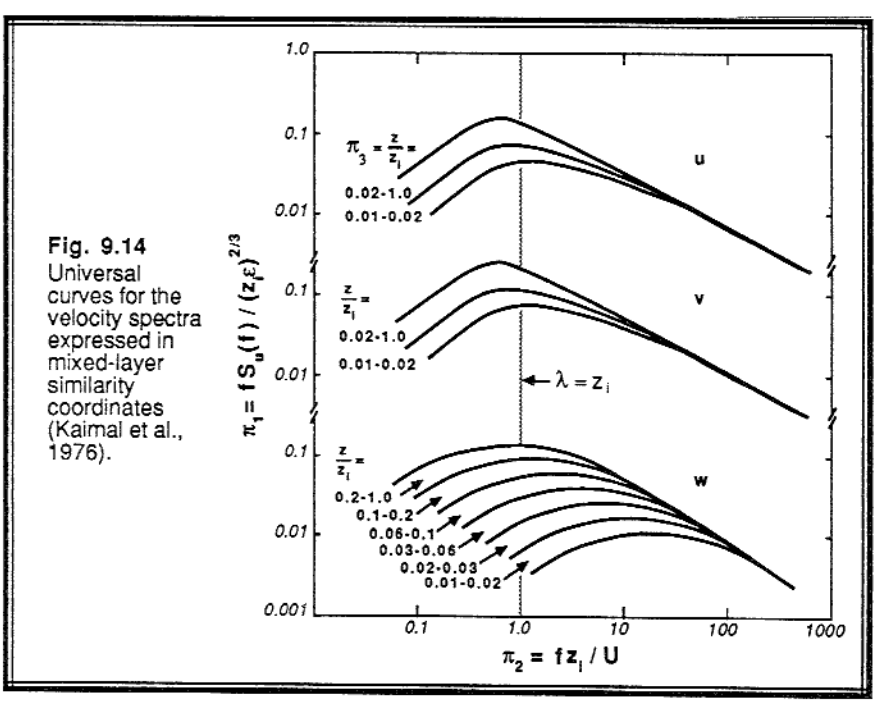

Fig. 9.14 Universal curves for the velocity spectra expressed in mixed-layer similarity coordinates (Kaimal et al., 1976).

analysis gives: $\pi_1 = f\, S_u(f) / (z_i\, \varepsilon)^{2/3}$, $\pi_2 = f\, z_i / \overline{U}$, and $\pi_3 = z / z_i$. These are plotted in Fig 9.14 for the u, v, and w components of the one-dimensional spectra (Kaimal, et al., 1976).

Notice that the peak in these curves corresponds to a wavelength approximately equal to the ML depth. This confirms our earlier statement that the most energetic eddies are the large ones that are produced on the scale of the boundary layer. In situations such as flow over complex terrain, new length scales might be introduced into the flow based on the scales of the terrain irregularities (Panofsky, et al., 1982).

9.10 Similarity Scaling Domains

In different parts of the boundary layer, we typically find that the nature of the flow is dependent on some scaling parameters, and not dependent on others. For example, in the surface layer we expect turbulence and mean profiles to be related to z/L, but in the ML we find that z/z_i is more appropriate than z/L. To help organize or knowledge about the relevant scaling parameters, Fig 9.15 relates parameters to identifiable parts of the ***unstable*** BL, while Fig 9.16 does the same for the ***stable*** BL.

In Fig 9.15a, the regions that are independent of L or z_i are indicated. In Fig 9.15b, the regions are listed along with the variables that are relevant for each region. We find

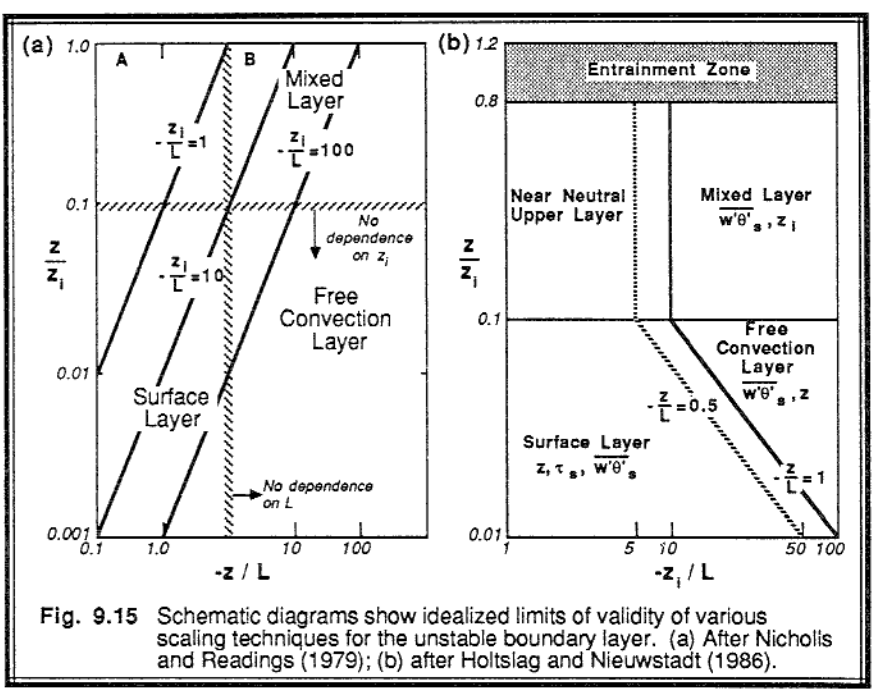

Fig. 9.15 Schematic diagrams show idealized limits of validity of various scaling techniques for the unstable boundary layer. (a) After Nicholls and Readings (1979); (b) after Holtslag and Nieuwstadt (1986).

that in addition to the ML and SL, there are two new regions that can be identified. One layer is the ***free convection layer*** that forms in strongly convective situations near the ground. It can be thought of as the region between the top of the SL and the bottom of the ML, where neither L nor z_i length scales are relevant. The other region is a ***near neutral upper layer*** that is similar to the residual layer except that it is still turbulent and still feeling the effects of the surface. These conditions might happen on a windy day with clear skies over land, where both buoyant and mechanical generation of turbulence are present. They might also exist in stratocumulus-topped mixed layers.

For stable conditions, Fig 9.16 shows a region in the upper right portion of the graph that corresponds to strongly stable air that is in the top of the SBL. Turbulence in this region is likely to be ***intermittent***, because of the strong stability suppressing turbulence. In the middle of the SBL is a region that might be continuously turbulent, but which is independent of height above ground and of surface fluxes. In this ***z-less*** region, only the magnitudes of the local fluxes are important. Below this region ***local scaling*** continues to be important for more neutral stability, but now the turbulence senses the bottom boundary and is dependent on z. Finally, adjacent to the ground is the usual surface layer, where surface fluxes and z are important. Note that the ***near neutral upper layer*** defined in this graph is within the SBL, and is not the residual layer that lies above the SBL.

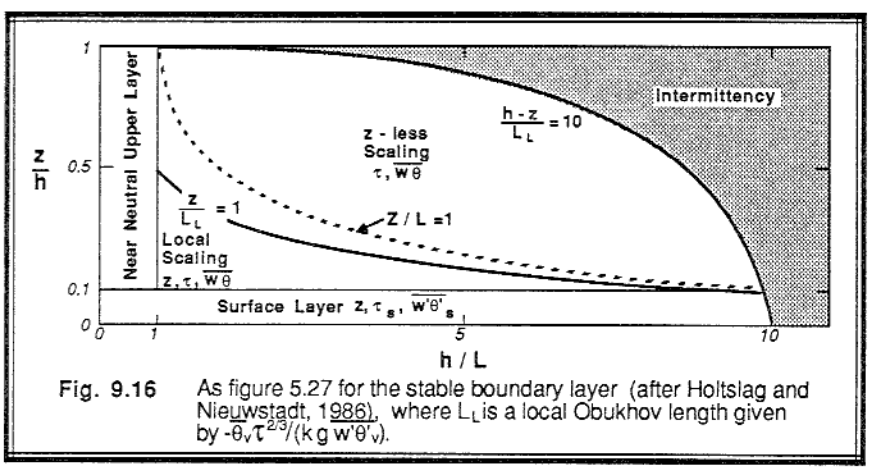

Fig. 9.16 As figure 5.27 for the stable boundary layer (after Holtslag and Nieuwstadt, 1986), where L_L is a local Obukhov length given by $-\theta_v \tau^{2/3}/(k\, g\, \overline{w'\theta'_v})$.

9.11 References

American Geophysical Union, 1969: Spectra of Meteorological Variables. *Radio Science*, **4**, No. 12, 1099-1397.

André, J.-C., and C. Blondin, 1986: On the effective roughness length for use in numerical 3-D models. *Bound.-Layer Meteor.*, **35**, 231-245.

Arya, S.P.S., 1981: Parameterizing the height of the stable atmospheric boundary layer. *J. Appl. Meteor.*, **20**, 1192-1202.

Benoit, R., 1977: On the integral of the surface layer profile-gradient functions. *J. Appl. Meteor.*, **16**, 859-860.

Berkowicz, R. and L.P. Prahm, 1984: Spectral representation of the vertical structure of turbulence in the convective boundary layer. *Quart. J. Roy. Meteor. Soc.*, **110**, 35-52.

Brost, R.A., J.C. Wyngaard and D.H. Lenschow, 1982: Marine stratocumulus layers. Part II: Turbulence budgets. *J. Atmos. Sci.*, **39**, 818-836.

Buckingham, 1914: On physically similar systems: illustrations of the use of dimensional analysis, *Phys. Rev.*, **4**, 345.

Busch, N.E., 1973: On the mechanics of atmospheric turbulence. *Workshop on Micrometeorology*. (Ed. by D.A. Haugen). Amer. Meteor. Soc., Boston. 1-65.

Businger, J.A., J.C. Wyngaard, Y. Izumi and E.F. Bradley, 1971: Flux profile relationships in the atmospheric surface layer. *J. Atmos. Sci.*, **28**, 181-189.

Caughey, S.J. and S.G. Palmer, 1979: Some aspects of turbulent structures through the depth of the convective boundary layer. *Quart. J. Roy. Meteor. Soc.*, **105**, 811-827.

Caughey, S.J. and C.J. Readings, 1974: The vertical component of turbulence in convective conditions. *Adv. in Geophys.*, **18A**, 125-130.

Caughey, S.J. and C.J. Readings, 1975: Turbulent fluctuations in convective conditions. *Quart. J. Roy. Meteor. Soc.*, **101**, 537-542.

Caughey, S.J., J.C. Wyngaard and J.C. Kaimal, 1979: Turbulence in the evolving stable boundary layer. *J. Atmos. Sci.*, **36**, 1041-1052.

Chamberlain, A.C., 1983: Roughness length of sea, sand and snow. *Bound. Layer Meteor.*, **25**, 405-409.

Charnock, H., 1955: Wind stress on a water surface. *Quart. J. Roy. Meteor. Soc.*, **81**, 639-640.

Deardorff, J.W., 1972: Numerical investigation of neutral and unstable planetary boundary layers. *J. Atmos. Sci.*, **29**, 91-115.

Deardorff, J.W., G.E. Willis and B.H. Stockton, 1980: Laboratory studies of the entrainment zone of a convectively mixed layer. *J. Fluid Mech.*, **100**, 41-64.

Dyer, A.J., 1974: A review of flux-profile relations. *Bound. Layer Meteor.*, **1**, 363-372.

Garratt,J.R., 1977: Review of drag coefficients over oceans and continents. *Mon. Wea. Rev.*, **105**, 915-929.

Gossard, E.E., R.B. Chadwick, W.D. Neff, and K.P. Moran, 1982: The use of ground-based Doppler radars to measure gradients, fluxes and structure parameters in elevated layers. *J. Appl. Meteor.*, **21**, 211-226.

Grant, A.L.M., 1986: Observations of boundary layer structure made during the 1981 KONTUR experiment. *Quart. J. Roy. Meteor. Soc.*, **112**, 825-841.

Hicks, B.B., P. Hyson and C.J. Moore, 1975: A study of eddy fluxes over a forest. *J. Appl. Meteor.*, **14**, 58-66.

Holtslag, A.A.M. and F.T.M. Nieuwstadt, 1986: Scaling the atmospheric boundary layer. *Bound.-Layer Meteor.*, **36**, 201-209.

Kaimal, J.C., J.C. Wyngaard, D.A. Haugen, O.R. Coté, Y. Izumi, S.J. Caughey, and

C.J. Readings, 1976: Turbulence structure in the convective boundary layer. *J. Atmos. Sci.*, **33**, 2152-2169.

Kaimal, J.C., J.C. Wyngaard, Y. Izumi and O.R. Coté, 1972: Spectral characteristics of surface layer turbulence. *Quart. J. Roy. Meteor. Soc.*, **98**, 563-589.

Kolmogorov, A.N., 1941: Energy dissipation in locally isotropic turbulence. *Doklady AN SSSR*, **32**, No. 1, 19-21.

Kondo, J. and H. Yamazawa, 1986: Aerodynamic roughness over an inhomogeneous ground surface. *Bound.-Layer Meteor.*, **35**, 331-348.

Lascer, A. and S.P.S. Arya, 1986: A numerical model study of the structure and similarity scaling of the nocturnal boundary layer. *Bound.-Layer Meteor.*, **35**, 369-386.

LeMone, M.A. and W.T. Pennell, 1976: The relationship of the trade wind cumulus distribution to subcloud layer fluxes and structure. *Mon. Wea. Rev.*, **104**, 524-539.

Lenschow, D.H., 1974: Model of the height variation of the turbulence kinetic energy in the unstable planetary boundary layer. *J. Atmos. Sci.*, **31**, 465-474.

Lenschow, D.H., J.C. Wyngaard, and W.T. Pennell, 1980: Mean field and second moment budgets in a baroclinic convective boundary layer. *J. Atmos. Sci.*, **37**, 1313-1326.

Lettau, H., 1969: Note on aerodynamic roughness-parameter estimation on the basis of roughness-element description. *J. Appl. Meteor.*, **8**, 828-832.

Mahrt, L. and J.-C. André, 1983: On the stratification of turbulent mixed layer. *J. Geophys. Res.*, **88**, 2662-2666.

Merry, M. and H.A. Panofsky, 1976: Statistics of vertical motion over land and water. *Quart. J. Roy. Meteor. Soc.*, **102**, 225-260.

Moeng, C.-H. and J.C. Wyngaard, 1984: Statistics of conservative scalars in the convective boundary layer. *J. Atmos. Sci.*, **51**, 3161-3169.

Monin, A.S. and A.M. Obukhov, 1954: Basic laws of turbulent mixing in the atmosphere near the ground. *Tr. Akad. Nauk., SSSR Geophiz. Inst.*, No. 24 (151), 1963-1987.

Nappo,C.J., Jr., 1977: Mesoscale flow over complex terrain during the Eastern Tennessee Trajectory Experiment (ETTEX). *J. Appl. Meteor.*, **16**, 1186-1196.

Nicholls, S., and C.J. Readings, 1979: Aircraft observations of the structure of the lower boundary layer over the sea. *Quart. J. Roy. Meteor. Soc.*, **105**, 785-802.

Nickerson, E.C. and V.E. Smiley, 1975: Surface layer and energy budget parameterizations for mesoscale models. *J. Appl. Meteor.*, **14**, 297-300.

Nieuwstadt, F.T.M., 1984: The turbulent structure of the stable, nocturnal boundary layer. *J. Atmos. Sci.*, **41**, 2202-2216.

Obukhov, A.M., 1941: Energy distribution in the spectrum of a turbulent flow. *Izvestiya AN SSSR, Ser. Geogr. Geofiz.*, No. 4-5, 453-466.

Panofsky, H.A., D. Larko, R. Lipschutz, G. Stone, E.F. Bradley, A.J. Bowen and J. Højstrup, 1982: Spectra of velocity components over complex terrain. Quart. J. Roy. Meteor. Soc., 108, 215-230.

Panofsky, H.A., H. Tennekes, D.H. Lenschow, and J.C. Wyngaard, 1977: the characteristics of turbulent velocity components in the surface layer under convective

conditions. *Bound.-Layer Meteor.*, **11**, 355-361.

Paulson, C.A., 1970: The mathematical representation of wind speed and temperature in the unstable atmospheric surface layer. *J. Appl. Meteor.*, **9**, 857-861.

Perry, R.H., C.H. Chilton and S.D. Kirkpatrick, (Eds.), 1963: *Perry's Chemical Engineer's Handbook, 4th Ed.*. McGraw Hill, NY. 2-87 to 2-90.

Smedman-Högström, A.-S., and U. Högström, 1978: A practical method for determining wind frequency distributions for the lowest 200 m from routine meteorological data. *J. Appl. Meteor.*, **17**, 942-954.

Smith, S.D., 1980: Wind stress and heat flux over the ocean in gale force winds. *J. Phys. Ocean.*, **10**, 709-726.

Sorbjan, Z., 1986: On similarity in the atmospheric boundary layer. *Bound. Layer Meteor.*, **34**, 377-397.

Sorbjan, Z., 1987: An examination of local similarity theory in the stably stratified boundary layer. *Bound.-Layer Meteor.*, **38**, 63-71.

Stull, R.B., 1983: Integral scales for the nocturnal boundary layer. Part I: Empirical depth relationships. *J. Clim. Appl. Meteor.*, **22**, 673-686.

Taylor, P.A., 1987: Comments and further analysis on effective roughness lengths for use in numerical 3-D models. *Bound.-Layer Meteor.*, **39**, 403-418.

Tennekes, H., 1973: Similarity laws and scale relations in planetary boundary layers. *Workshop on Micrometeorology* (Ed., D.A. Haugen), Am. Meteor. Soc., 177-216.

Tennekes, H., 1976: Fourier-transform ambiguity in turbulence dynamics. *J. Atmos. Sci.*, **33**, 1660-1663.

Tennekes, H., 1982: Similarity relations, scaling laws and spectral dynamics. *Atmospheric Turbulence and Air Pollution Modelling*. (Ed. by F.T.M. Nieuwstadt and H.van Dop). Reidel. 37-68.

Thompson, R. S., 1978: Note on the aerodynamic roughness length for complex terrain, *J. Appl. Meteor.*, **17**, 1402-1403.

Webb, E.K., 1982: Profile relationships in the superadiabatic surface layer. *Quart. J. Roy. Meteor. Soc.*, **108**, 661-688.

Whitaker, S., 1968: *Introduction to Fluid Mechanics*. Prentice-Hall, Englewood Cliffs. 457pp.

Wyngaard, J.C., 1973: On surface layer turbulence. *Workshop on Micrometeorology*. (Ed. D.A. Haugen). Am. Meteor. Soc. 101-148.

Wyngaard, J.C. and R.A. Brost, 1984: Top-down and bottom-up diffusion of a scalar in the convective boundary layer. *J. Atmos. Sci.*, **41**, 102-112.

Wyngaard, J.C. and O.R. Coté, 1971: Budgets of turbulent kinetic energy and temperature variance in the atmospheric surface layer. *J. Atmos. Sci.*, **28**, 190-201.

Wyngaard, J.C., O.R. Coté, and Y. Izumi, 1971: Local free convection, similarity, and the budgets of shear stress and heat flux. *J. Atmos. Sci.*, **28**, 1171-1182.

Yamada, T., 1976: On the similarity functions A, B, and C of the planetary boundary layer. *J. Atmos. Sci.*, **33**, 781-793.

Zhou, M.Y., D.H. Lenschow, B.B. Stankov, J.C. Kaimal, and J.E. Gaynor, 1985: Wave and turbulence structure in a shallow baroclinic convective boundary layer and overlying inversion. *J. Atmos. Sci.*, **42**, 47-57.

9.12 Exercises

1) Suppose that the wind speed, $\overline{M}$, near the surface at night is a function of $g/\overline{\theta_v}$, $\overline{w'\theta_v'}$, $\partial z/\partial x$, $\partial\overline{\theta_v}/\partial z$, z_o, and $\overline{U_g}$. Use Buckingham Pi dimensional analysis to determine the relevant Pi groups.

2) You were recently hired to make background environmental measurements at the site of a proposed power plant. The site happens to be of uniform roughness in all directions, and the land use in this area does not change with the seasons (i.e., no harvesting, logging, or other changes).
a) On one particular overcast day, you measured the following wind speed profile as a function of height using your instrumented 100 m tower and a rawinsonde that you launched: Find z_o and u_*.

z (m)	1	10	100	200	500	1000
$\overline{M}$ (m/s)	1	2	3	3	3	3

b) Later in the year, you sold the tall tower and donated the funds to your favorite meteorological charity. But your contract with the power company still required you to make background measurements. Therefore, you erected a shorter, 10 m tower at the same site. Then came another overcast day with the wind from the same direction as before. You measured a speed of 4 m/s at the top of your short tower. What is value of u_* on this day, and what is the wind speed at z = 50 m (the height of the proposed smoke stack from the power plant)?

3) If an orchard is planted with 1000 trees per square kilometer, where each tree is 4 m tall and has a vertical cross-section area (effective silhouette to the wind) of 5 m^2, what is the aerodynamic roughness length? Assume d=0.

4) Given the following wind speed data for a neutral surface layer, find the roughness length (z_o), displacement distance (d), and friction velocity (u_*):

z(m):	5	8	10	20	30	50
$\overline{M}$(m/s):	3.48	4.43	4.66	5.50	5.93	6.45

5) Suppose that the following was observed on a clear night (no clouds) over farmland having z_o = 0.067 m (assume k = 0.4), L (Obukhov length) = 30 m, u_* = 0.2 m/s. Find and plot $\overline{M}$ as a function of height up to 50 m.

6) a) If the displacement distance is zero, find z_o and u_*, given the following data in statically neutral conditions at sunset:

z(m)	M(m/s)
1	4.6
3	6.0
10	7.6
30	9.0

b) Later in the evening at the same site, $\overline{w'\theta_v'}$= -0.01 K m/s, and $g/\overline{\theta_v}$ = 0.03333 m s^{-2} K^{-1}. If u_* = 0.3 m/s, calculate and plot the wind speed profile ($\overline{U}$ vs z) up to z = 50 m.

7) Assume that the following variables are relevant for flow over an isolated hill:

$(g/\overline{\theta_v})\,\partial\overline{\theta_v}/\partial z$ = stability parameter

$\overline{M}$ = wind speed
D = diameter of hill
H = height of hill

Use Buckingham Pi methods to find the dimensionless groups for this problem.

8) Given: A SBL with z_o = 1 cm, $\overline{\theta_v}$ (at z = 10 m) = 294 K, $\overline{w'\theta_v'}_s$ = - 0.02 K·ms^{-1}, u_* = 0.2 m/s, k = 0.4. Plot the mean wind speed as a function of height on a semi-log graph for $1 \le z \le 100$ m.

9) Given the following wind speeds measured at various heights in a neutral boundary layer, find the aerodynamic roughness length (z_o), the friction velocity (u_*), and the shear stress at the ground (τ). What would you estimate the wind speeds to be at 2 m and at 10 cm above the ground? Use semi-log paper. Assume that the von Karman constant is 0.35 .

z (m)	U (m/s)
2000	10.0
1000	10.0
500	9.5
300	9.0
100	8.0
50	7.4
20	6.5
10	5.8
4	5.0
1	3.7

10) Consider the flow of air over a housing development with no trees and almost identical houses. In each city block (0.1 km by 0.2 km), there are 20 houses, where each house has nearly a square foundation (10 m on a side) and has an average height of 5 m. Calculate the value of the surface stress acting on this neighborhood when a wind speed of 10 m/s is measured at a height of 20 m above ground in statically neutral conditions. Express the stress in Pascals.

11) Derive an expression for the kinematic heat flux ($\overline{w'\theta'}$) in terms of the dimensionless wind shear (ϕ_M) and the dimensionless lapse rate (ϕ_H). Then, given a wind shear of

0.02 1/s and a lapse rate of -0.012 K/m at a height of 20 m above ground, calculate the value of the heat flux at that height using Businger's flux-profile relationships. Assume a mean potential temperature of 21 °C. To simplify your calculations, recall that z/L is approximately equal to the Richardson number for unstable conditions.

12) State some reasons why one might need to use geostrophic drag relationships.

13) Use the definition of the drag coefficient along with the neutral log wind profile equation to prove that $C_{DN} = k^2 \ln^{-2}(z/z_o)$.

14) Given the definition for eddy diffusivity $\overline{u'w'} = - K \partial\overline{U}/\partial z$, solve for K as a function of height in the neutral surface layer, assuming a log wind profile.

15) Given the answer from the previous question, and the definition for Ekman layer depth $h_E = (2 \pi^2 K/f_c)^{1/2}$, show that the Ekman layer depth is proportional to u_*/f_c.

16) Given the following variables and their dimensions:

z	height	L
g/θ	buoyancy parameter	L T^{-2} K^{-1}
TKE	turbulence KE per unit mass	L^2 T^{-2}
Zi	depth of the mixed layer	L
w'θ'	surface kinematic heat flux	L T^{-1} K

Perform a dimensional analysis to find Pi groups for z and TKE, using the remaining variables as the primary variables.

17) Using the Businger-Dyer flux-profile relationship for statically stable conditions:

a) Derive an equation for the drag coefficient, C_D, as a function of the following 4 parameters:

z : height above ground
z_o : roughness length
L : Obukhov length
k : von Karman constant (= 0.35)

b) Find the resulting ratio of C_D/C_{DN} , where C_{DN} is the neutral drag coefficient.

c) Given z = 10 m and z_o = 10 cm, calculate and plot C_D/C_{DN} for a few different values of stability: $0 < z/L < 1$. How does this compare with Fig 7.10a?

18) Given the surface layer profile plotted at right: List 2 different reasons why the profile might look like this.

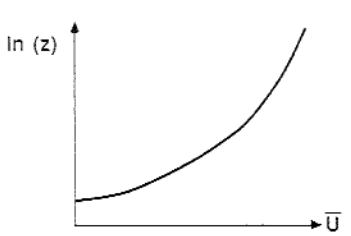

19) Given the following wind profile:

z (m)	U (m/s)
0.3	5.0
0.7	6.0
1.0	6.4
2.0	7.2
10.0	9.0
50.0	10.0
100.0	10.2
1000.0	10.4

and density $\overline{\rho} = 1.25$ kg/m^3. Assume the displacement distance d = 0.

a) Find z_o.

b) Find u_*

c) Find the surface stress (in units of N/m^2)

d) Given a different day over the same land surface, but with $z/L = -1.0$ and $u_* =$ 1.0 m/s. Is the wind fast enough to 'knock your socks off' ? (Assume that sock height = 25 cm, and that it takes a wind speed of 10 m/s at that height to 'knock your socks off'.)

20) Given: $\partial\overline{U}/\partial z = u_* / k z$, and $K_m = k z u_*$ for simplicity (although this is not necessarily a neutral surface layer). Given also: $u_* = 0.3$ m/s, $\overline{\theta} = 280 + 1.0 \ln(z/z_o)$ in degrees Kelvin, and $z_o = 1$ cm.

a) Find $\partial\overline{\theta}/\partial t$.

b) Calculate the numerical value of the flux Richardson number.

c) Is the flow turbulent? Why?

21) During the night, assume that the TKE is a function of the following parameters:

(z_o, z, $g/\overline{\theta}$, $\Delta\overline{\theta}_s$, $\overline{U_g}$, ν) where ν has units of length times velocity.

Use dimensional analysis to find the dimensionless PI groups.

22) Given the following wind profile in statically neutral conditions:

z (m)	$\overline{U}$ (m/s)
0.95	3
3.0	4
9.5	5
30.0	6

Find the numerical value of:

a) z_o

b) u_*

c) K_m at 3 m

d) C_D.

23) Given $z_o = 1$ cm = constant and $u_* = 0.25$ m/s = constant. Find and plot the ratio of 10 m mean wind speed for diabatic conditions to that for neutral conditions, as a function of stability for $0 \le (z/L) \le 2.0$. Briefly describe the significance of your result.

24) It has been suggested that in regions of strong static stability the lower (long wavelength, small wavenumber) end of the inertial subrange occurs at a wavenumber, κ_b, given by $\kappa_b = N_{BV}^{2/3} \varepsilon^{-1/2}$, where N_{BV} is the Brunt-Vaisala frequency, and ε is the turbulence dissipation rate. Use dimensional analysis to arrive at the above expression.

25) Given the following mean wind speed profile, find the roughness length (z_o) and the friction velocity (u_*). Assume that the surface layer is statically neutral, and that the displacement distance $d = 0$. Use $k = 0.35$.

z (m)	$\overline{M}$ (m/s)
1	3.0
3	4.0
10	5.0
20	5.6
50	6.4
100	6.8
500	7.0
1000	7.0

26) Knowing the shear ($d\overline{M} / dz$) at any height z is sufficient to determine the friction velocity (u_*) for a neutral surface layer:

$$u_* = k\ z\ d\overline{M}/dz$$

If, however, you do not know the local shear, but instead know the value of the wind speed $\overline{M}_2$ and $\overline{M}_1$ at the heights z_2 and z_1 respectively, then you could use the following alternative expression to find u_*: $u_* = k Z^* \Delta\overline{M} / \Delta z$

Derive the exact expression for Z^*.

27) Given the following wind speed data for a neutral surface layer, find the roughness length (z_o), the displacement distance (d), and the friction velocity (u_*):

z (m)	$\overline{M}$ (m/s)
5	3.48
8	4.34
10	4.66
20	5.50
30	5.93
50	6.45

28) Suppose that you have made micrometeorological measurements over a wheat field, where $z_o = 1$ cm. Assume $(g/\overline{\theta}) = 0.0333$ m/(s^2 K).

a) One afternoon, $u_* = 0.36$ m/s and $\overline{w'\theta'} = 0.20$ K m/s at the surface. What is the value of the Obukhov length? Plot the mean wind speed as a function of height from the surface to 50 m.

b) Later, during the night when $\overline{w'\theta'} = -0.05$ K m/s at the surface, you measured the same wind speed at a height of 20 m as you observed during the afternoon (from your answer to part a). Find the friction velocity u_* and the Obukhov length (L) for this nighttime situation, and plot the resulting wind speed profile between the surface and 50 m .

29) a) Given the following was observed over farmland on an overcast day:

$u_* = 0.4$ m/s , $d = 0$, $\overline{M} = 5$ m/s at $z = 10$ m . Find z_o .

b) Suppose that the following was observed on a clear night (no clouds) over the same farmland: $L = 30$ m, $u_* = 0.2$ m/s . Find $\overline{M}$ at $z = 1$, 10, and 20 m.

c) Plot the wind speed profiles from (a) and (b) on semi-log graph paper.

30) Given the following data: $\overline{w'\theta'} = 0.2$ K m/s, $z_i = 500$ m, $g/\overline{\theta} = 0.0333$ m s^{-2} K^{-1} $u_* = 0.2$ m/s, $k = 0.4$, $z_o = 0.01$ m, $z = 6$ m

Find:

a) L (the Obukhov length)

b) z/L

c) $\partial\overline{U}/\partial z$ at z=6 m. (Hint: use diabatic surface layer similarity)

31) The wind speed = 3 m/s at a height of 4 m. The ground surface has a roughness length of $z_o = 0.01$ m. Find the value of u_* for

a) A convective daytime boundary layer where Ri = -0.5 .

b) A nocturnal boundary layer where Ri = 0.5 .